TURN PERFORMANCE AND FLIGHT DYNAMICS OF A PTEROSAUR AND A PTEROSAUR-INSPIRED VARIABLE-PLACEMENT VERTICAL TAIL AIRCRAFT

By

BRIAN C. ROBERTS

A THESIS PRESENTED TO THE GRADUATE SCHOOL
OF THE UNIVERSITY OF FLORIDA IN PARTIAL FULFILLMENT
OF THE REQUIREMENTS FOR THE DEGREE OF
MASTER OF SCIENCE

UNIVERSITY OF FLORIDA

2009

I dedicate this thesis to all of my teachers, from grade school to grad school

ACKNOWLEDGMENTS

Thanks to Dr. Lind for putting me on this out-of-the-ordinary and yet fully engaging project and for helping me along the way. A very appreciative thanks to Dr. Sankar Chatterjee for all of his paleontological insight. I want to thank all of my labmates and classmates for any advice and ideas I received through contact with them. I especially want to thank Daniel Grant for getting me started on AVL and for all of his assistance along the way.

TABLE OF CONTENTS

LIST OF TABLES

LIST OF FIGURES

Abstract of Thesis Presented to the Graduate School
of the University of Florida in Partial Fulfillment of the
Requirements for the Degree of Master of Science

TURN PERFORMANCE AND FLIGHT DYNAMICS OF A PTEROSAUR AND
A PTEROSAUR-INSPIRED VARIABLE-PLACEMENT VERTICAL TAIL AIRCRAFT

By

Brian C. Roberts

May 2009

Chair: Rick Lind
Major: Aerospace Engineering

Mission performance for small aircraft is often dependent on turn radius. Various biologically-inspired concepts have demonstrated that performance can be improved by morphing the wings in a manner similar to birds and bats; however, morphing of the vertical tail has received less attention because neither birds nor bats have an appreciable vertical tail. In contrast, pterosaurs have a large vertical crest on their heads that could have improved their flight performance to assist in tasks necessary for survival. This thesis investigates the flight dynamics of a pterosaur and analyzes the aerodynamic and weight effects of a pterosaur's head on performance. Additionally, aerodynamic interactions between the crest and a pterosaur's wing-sweep morphing capabilities are analyzed. The thesis uses these results to design an aircraft model that incorporates a morphing of the vertical tail based on the cranial crest of a pterosaur. The flight dynamics of the aircraft model demonstrate a reduction in turn radius of 13% when placing the tail over the nose in comparison to a traditional aft-placed vertical tail.

CHAPTER 1
INTRODUCTION

1.1 Motivation

Urban surveillance and sensor emplacement is an area of interest for both military and civilian applications. In both wartime and emergency disaster situations, authorities need as much information as possible in a short amount of time to make good decisions as to how to proceed to solve the situation. A miniature aerial vehicle (MAV) is an ideal platform to deliver sensors to the area to obtain information. Consider this mission for an urban operation:

Phase I: The vehicle flies from a launch site into an urban area using high-altitude cruise flight. The vehicle then descends rapidly below the building rooflines. It traverses a region through immersive obstacles by agile maneuvering until a target site is identified.

Phase II: It flies around the region to provide aerial close-proximity sensing. The vehicle circles the area monitoring the region of interest and processing the terrain to find a good place to land to investigate the target more closely. Onboard computers plan the vehicle's path from its landing site to the target to optimize obstacle avoidance and sensor coverage

Phase III: The vehicle lands. It then walks from its landing site to the target to gather more information. The vehicle may need to stay hidden to complete its mission, or it may have to avoid large obstacles. The physical orientation is shifted to maximize information gathering and maintain sensor coverage while remaining on this path.

Phase IV: The vehicle takes off using a high-lift design. It successfully navigates its way out of the urban terrain and returns to base.

A number of challenges are elucidated in this mission scenario. The individual segments have unique features that must be considered; however, the combination of all segments into the total mission drastically increases the aspects for which the design must account.

- The mission requires a high degree of maneuverability. Densely spaced buildings, light poles, wires, antennas, as well as moving people, cars, machinery and other fixtures of the urban landscape all reduce the navigable pathways from one location to another. The flight mode will require small-radius turns, high-speed dives, precise landings, and trim at high angle of attack and high angle of sideslip.

- The mission requires the system to be robust with respect to aerodynamic disturbances. The narrow gaps between buildings, sometimes referred to as urban canyons, channel airflows through them, creating pockets of high velocity wind next to pockets of negligible airflow. The obstacles that make navigation so difficult also have the added effect of disrupting the airflow and creating large amounts of unpredictable turbulence and vortices.

- The vehicle must be capable of sophisticated path planning to find a route to the target and the best place from which to observe it. It must plan its information-gathering path both in flight and on the ground, so multiple algorithms may be required.

- The phases require different types of locomotion. The first two phases require flight, the second phase uses walking, and the third phase requires the vehicle to be able to takeoff from the ground, on what might be rough terrain. The mechanics for such locomotive variety can be highly specialized and dependent on a particular configuration.

- A series of transitions between the types of locomotion must be performed. The vehicle must maintain terrestrial stability when transitioning to and from the walking phase.

- The sensor emplacement must maintain coverage. The sensor must be put into a desired location but also that sensor must be oriented towards the target. Techniques beyond sensor gimbaling must be adopted to avoid self-occlusion and other issues. The sensors must also be reduced in weight to reduce the size and necessary speed the vehicle must maintain.

- The vehicle must be able to survive an entire operation. The choice of materials is extremely important in that the vehicle must not be too fragile. Obviously a series of landings, either on land or water, can put excessive strain on the vehicle structure, making ruggedness and durability of construction vitally important.

- The vehicle must have a level of autonomy that facilitates use by a non-specialist operator. The vast majority of warfighters in theater and emergency personnel are not expert remote-aircraft pilots; consequently, the transition of this design to military and civilian use will depend on its ability to be effectively used by a wide set of operators.

Some of these requirements have already been satisfied, while others are still lacking.

Great advances by controls engineers in autopilot software have made waypoint navigation fairly simple in the absence of obstacles, and path planning for obstacle avoidance and sensor coverage has advanced. Many sensors have been greatly reduced in size and weight to permit their inclusion on smaller, more agile aircraft.

Robotics has advanced to the point that building vehicles that are capable of both flying and walking is a possibility, but the transitions will prove to be the most difficult part. The task of flying and then walking can be accomplished in a very limited sense using current technology; however, the return to flight has not yet matured.

Efforts to make MAV's more mission capable have made some gains. Robust design methods and materials continue to find new ways to make sophisticated systems more reliable in the field. Computer science is still trying to make user interfaces more intuitive to make flying vehicles accessible to a wider range of users. Multi-touchscreen technology represents a large step forward in making the upper level control of vehicles instinctive. However, even though MAV's have been flown for years as demonstration tools, they have not yet been proven mission capable.

Most important to this thesis is the lack of vehicle capability for urban navigation. More than any other reason, MAV's have failed to realize their potential because they have not attained the combination of high-performance maneuverability combined with a robustness with respect to disturbances.

The design community is rapidly adopting biologically-inspired concepts as a valuable paradigm to enhance mission capability. The general concept notes that biological systems are often able to perform maneuvers that can not be duplicated by engineered systems based on traditional designs; consequently, the aspects associated with that capability for biological systems could be incorporated into the engineered systems to attain similar capabilities. The chemical processes, such as energy and reproduction, are being studied but remain challenging; however, the issues of shape changing and mass distribution through morphing are often realizable using off-the-shelf technology.

A significant effort into morphing was pursued by NASA as an effort to adopt avian concepts for aircraft in the hopes of improving performance (1). That project studied various aspects of morphing design but focused primarly on materials technology. A vehicle was never realized through this project; however, some lessons about morphing were fundamental to the later success of the Active Aeroelastic Wing (2). A morphing program was also initiated by DARPA with strong emphasis on biologically-inspired design (3). That program also placed primary focus on materials and associated structural technologies; however, it has a pair of contractors building vehicles in hopes of a flight demonstration.

The University of Florida is acknowledged for its advancement into biologically-inspired design through an extensive flight program of morphing micro air vehicles (4–7). Their designs include articulated wings that mimic the shoulders and elbows of birds to vary both the dihedral and sweep. In each case, the designs were limited to concepts inspired by birds and restricted to structural modifications to the wings.

Additionally, many studies into morphing aircraft have focused on the steady-state benefits of altering a configuration for issues such as fuel consumption (8), range and endurance (9), cost and logistics (10), actuator energy (11), maneuverability (12), and airfoil requirements (13). Additionally, aeroelastic effects have been often studied relative to maximum roll rate (14),(15),(16) and actuator loads (17).

1.2 Problem Statement

This paper introduces a biologically-inspired concept from pterosaurs to enhance mission performance; specifically, an aircraft is designed to incorporate a variable-placement vertical tail that is similar in nature to the cranial crest of the pterosaur (18). This design allows the vertical tail to be able to move forward, like the pterosaur, or aft, like a traditional aircraft, along the fuselage to affect the turn performance. The flight dynamics are analyzed to note that moving the vertical tail over the nose reduces the turn radius by 13%.

The goal of this research is to find ways to use the vertical tail to improve maneuverability and performance aspects of MAV flight while still maintaining stability and controllability to minimize the impact of disturbances on the vehicle. The research investigates not only the direct impact of the vertical tail on the vehicle's dynamics, but also the interactions between the vertical tail and other flight configuration changes as well as secondary effects from flight conditions that may change as a result of the vertical tail.

The vertical tail's deflection angle is an obvious place to start to examine the role of this control surface. The vertical tail is deflected at a range of angles, and the resulting changes in trimmed flight conditions and linear dynamics are examined.

Vertical tail placement is also varied to try to find new ways to manipulate the control surface to create the desired performance improvements. Placement along both the longitudinal (front to back) and vertical (top to bottom) axes is investigated.

Wing sweep morphing is also included to provide another dimensionality to the research matrix. Both additive and reductive trends are noted between vertical tail deflection and morphing configuration.

1.3 Contribution

This thesis contributes several discoveries in the field of small aircraft dynamic effects due to vertical tail configuration.

- Research demonstrates trimmed turn performance improvements with varied vertical tail placement. An aircraft model shows reductions in turn radius and increases in turn rate when its vertical tail is placed forward of its center of mass and deflected by significant angles.
- Research indicates that longitudinal position of the vertical tail has a large effect on trimmed flight conditions, but that its vertical placement affects only the dynamics. This discovery will give aircraft designers insight into how to create a higher performance vehicle while avoiding unnecessary actuation.
- Research shows a dramatic increase in potential trimmed flight configurations when varied vertical tail placement is combined with morphing. Such morphing also provides a greater range of possible trimmed flight dynamics to assist in navigation, disturbance rejection, and sensor pointing.

- Research yields insights into how a pterosaur flew, thereby giving aircraft researchers another model on which to base small aircraft designs for urban surveillance missions.

CHAPTER 2
BACKGROUND

2.1 Axis and Moment Definitions

This thesis will discuss aircraft configuration and biological flight vehicle configuration extensively. Thus, it is vital that the reader understands the terms used to describe the vehicle's geometry .

- The axis that runs from nose to tail of an aircraft is referred to as the longitudinal axis, and its positive direction points out the nose of the vehicle. This axis is analogous to the anteroposterior axis of biological organisms and is orthogonal to the transverse plane. Roll rotation (also referred to as banking) occurs about this axis, causing one wing to move higher and the other to move lower (19). Positive roll moves the right wing down and the left wing up.

- The axis that lies orthogonal to the untwisted wing surface area is called the vertical axis, and its positive direction points out the right wing of the aircraft. Its comparative axis in anatomical terms is the dorsoventral axis and is orthogonal to the coronal plane. Rotation about this axis is called yaw, and causes the nose to move left or right (19). Positive yaw rotates the nose of the vehicle to the right.

- The axis that intersects both of the aircraft's wingtips is the lateral axis, and its positive direction points out the bottom of the aircraft. This axis is similar to the anatomical left-right axis and is orthogonal to the sagittal plane. An aircraft pitch is a rotation about this axis causing the nose to go up or down (19). Positive pitch rotates the nose of the vehicle up.

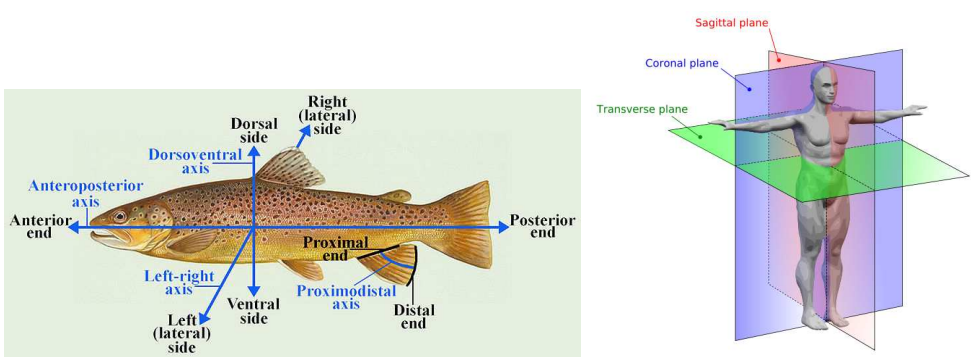

Figure 2-1. Diagram of Anatomical Axes and Planes

These definitions describe a body-fixed coordinate system. The direction of airflow past a vehicle rarely coincides with one of the body axes, and thus, belongs in its own

coordinate system. It is necessary to describe the wind axis in terms of the body-fixed axes (19).

$$
\begin{aligned}
&V_B = [u \;\; v \;\; w]^T \\
&u = magnitude\ of\ wind\ vector\ on\ body\ longitudinal\ axis \\
&v = magnitude\ of\ wind\ vector\ on\ body\ lateral\ axis \\
&w = magnitude\ of\ wind\ vector\ on\ body\ vertical\ axis
\end{aligned}
\tag{2–1}
$$

Two rotations are required to align the body's longitudinal axis with the wind axis. The first rotation is called the angle of sideslip, β, and aligns the aircraft's longitudinal axis with the wind axis in the coronal plane. Positive β points the nose to the left of the oncoming airflow. The second rotation is referred to as the angle of attack, α, and aligns the longitudinal axis with the wind axis in the sagittal plane. A positive α points the nose above the airflow (19).

$$
\begin{aligned}
\alpha &= \tan^{-1} \tfrac{w}{u} \\
\beta &= \sin^{-1} \tfrac{v}{V}
\end{aligned}
\tag{2–2}
$$

2.2 Aircraft Control Effectors

Aircraft use several types of control effectors to influence both forces and moments on the vehicle.

- A rudder is a control surface that controls the yawing moment of the aircraft. A rudder is usually a vertical control surface that is placed parallel to the vertical axis of the aircraft at a distance from the center of mass along the longitudinal axis (20).
- Elevators are control surfaces that control the pitching moment on the aircraft. Typically elevators are horizontal control surfaces located away from the center of mass along the longitudinal axis to be more effective at producing the moments that it controls. Elevators also move symmetrically to produce a uniform pitching moment rather than a roll moment (20).
- Ailerons are control surfaces that affect the rolling moment about the fuselage of the vehicle. Typically ailerons are horizontal control surfaces placed away from the center of mass along the aircraft's lateral axis. Ailerons also move asymmetrically

to produce an identical increase in lift on one wing and decrease in lift on the other. This combination of forces produces a pure roll moment with minimal pitch moment or lifting effects (20).

- Aircraft also use flaps to produce lift forces (orthogonal to the wing surface) and drag forces (parallel to the direction of airflow over the vehicle). Such control surfaces are usually placed along the lateral axis and move symmetrically to produce a net force effect with little moment (20).

2.3 Aircraft Equations of Motion

The full equations of motion of an aircraft are large nonlinear equations, ill-suited for this research (19).

$$
\begin{aligned}
&m(\dot{u} + qw - rv) = -mg\sin\Theta + (-D\cos A + L\sin A) + T\sin\Phi_T \\
&m(\dot{v} + ru - pw) = mg\sin\Phi\cos\Theta + F_{A_y} + F_{T_y} \\
&m(\dot{w} + pv - qu) = F_{G_z} + F_{A_z} + F_{T_z} \\
&L = p\dot{I}_x - qrI_y + qrI_z + (pr - \dot{q})I_{xy} - (pq + \dot{r})I_{xz} + (r^2 - q^2)I_{yz} + p\dot{I}_x - q\dot{I}_{xy} - r\dot{I}_{xz} \\
&M = prI_x + \dot{q}I_y - prI_z - (qr - \dot{p})I_{xy} + (p^2 - r^2)I_{xz} + (pq - \dot{r})I_{yz} + q\dot{I}_y - p\dot{I}_{xy} - r\dot{I}_{yz} \\
&N = -pqI_x + pqI_y + \dot{r}I_z + (q^2 - p^2)I_{xy} + (qr - \dot{p})I_{xz} - (pr + \dot{q})I_{yz} + r\dot{I}_z - p\dot{I}_{xz} - q\dot{I}_{yz} \\
&\dot{\phi} = p + q(\sin\phi + r\cos\phi)\tan\theta \\
&\dot{\theta} = q\cos\phi - r\sin\phi \\
&\dot{\psi} = (q\sin\phi + r\cos\phi)\sec\theta \\
&\dot{x}_{E_B} = u_B\cos\theta\cos\psi + v_B(\sin\phi\sin\theta\cos\psi - \cos\phi\sin\psi) + w_B(\cos\phi\sin\theta\cos\psi + \sin\phi\sin\psi) \\
&\dot{y}_{E_B} = u_B\cos\theta\sin\psi + v_B(\sin\phi\sin\theta\sin\psi - \cos\phi\cos\psi) + w_B(\cos\phi\sin\theta\sin\psi + \sin\phi\cos\psi) \\
&\dot{z}_{E_B} = -u_B\sin\theta + v_B(\sin\phi\cos\theta) + w_B\cos\phi\cos\theta
\end{aligned}
\tag{2–3}
$$

Instead, the aircraft will be assumed to follow linearized equations of motion about a steady-state trim condition (19).

$$
\begin{aligned}
&x_0 + \Delta x - mg(\sin\theta_0 + \Delta\theta\cos\theta_0) = m\Delta\dot{u} \\
&y_0 + \Delta y + mg\phi\cos\theta_0 = m(\Delta\dot{v} + u_0\Delta r) \\
&z_0 + \Delta z + mg(\cos\theta_0 - \Delta\theta\sin\theta_0) = m(\dot{\Delta}w - u_0\Delta q) \\
&L_0 + \Delta L = I_x\Delta\dot{p} - I_{zx}\Delta\dot{r} \\
&M_0 + \Delta M = I_y\Delta\dot{q} \\
&N_0 + \Delta N = -I_{zx}\Delta\dot{p} + I_z\Delta\dot{r} \\
&\dot{\theta}_0 + \Delta\dot{\theta} = \Delta q \\
&\dot{\phi}_0\Delta\dot{\phi} = \Delta p + \Delta r\tan\theta_0 \\
&\dot{\psi}_0\Delta\dot{\psi} = \Delta r\sec\theta_0 \\
&\dot{x}_{E_0} + \Delta\dot{x}_E = (u_0 + \Delta u)\cos\theta_0 - u_0\Delta\theta\sin\theta_0 + \Delta w\sin\theta_0 \\
&\dot{y}_{E_0} + \Delta\dot{y}_E = u_0\Psi\cos\theta_0 + \Delta v \\
&\dot{z}_{E_0} + \Delta\dot{z}_E = -(u_0 + \Delta u)\sin\theta_0 - u_0\Delta\theta\cos\theta_0 + \Delta w\cos\theta_0
\end{aligned}
\tag{2–4}
$$

The forces and moments are assumed to balance at the trim condition, allowing the equations to be manipulated to reveal linear equations for the incremental changes in those forces and moments (19).

$$
\begin{aligned}
\Delta X &= X_u \Delta u + X_w w + \Delta X_c \\
\Delta Y &= Y_v v + Y_p p + Y_r r + \Delta Y_c \\
\Delta Z &= Z_u \Delta u + Z_w w + Z_{\dot{w}} \dot{w} + Z_q q + \Delta Z_c \\
\Delta L &= L_v v + L_p p + L_r r + \Delta L_c \\
\Delta M &= M_u \Delta u + M_{\dot{w}} \dot{w} + \Delta M_c \\
\Delta N &= N_v v + N_p p + N_r r + \Delta N_c
\end{aligned}
$$

$$
\begin{aligned}
X &= force\ in\ longitudinal\ axis,\ positive\ points\ out\ of\ the\ nose \\
Y &= force\ in\ lateral\ axis,\ positive\ points\ out\ of\ right\ wing \\
Z &= force\ in\ vertical\ axis,\ positive\ points\ toward\ ground \\
L &= moment\ about\ longitudinal\ axis,\ positive\ rolls\ right\ wing\ down \\
M &= moment\ about\ lateral\ axis,\ positive\ pitches\ nose\ up \\
N &= moment\ about\ vertical\ axis,\ positive\ yaws\ nose\ to\ right \\
p &= roll\ rate = \dot{\phi} - \dot{\psi} \sin \theta_o \\
q &= pitch\ rate = \Delta \dot{\theta} \\
r &= yaw\ rate = \frac{\dot{\psi}}{\sec \theta_o}
\end{aligned}
\tag{2–5}
$$

2.4 Static Stability

Aircraft have three important static stability coefficients that affect the changes in moments seen in Equation 2–5.

The first coefficient indicates if the aircraft is longitudinally stable. This coefficient, C_{m_α}, is the derivative of the pitch moment with respect to changes in the aircraft's angle of attack. A negative value for C_{m_α} is stable because a positive angle of attack is nose-up and a positive pitch moment is also nose-up. So, a negative C_{m_α} produces a nose-down pitching moment when the nose is deflected upward, restoring the aircraft to its trim condition (21).

$$C_{m_\alpha} = \frac{\delta M}{qS_w c \delta\alpha} \tag{2–6}$$

The second static stability coefficient yields the directional stability of the aircraft. C_{n_β} is the derivative of the yaw moment with respect to angle of sideslip. A positive C_{n_β} is stable because a positive angle of sideslip points the nose to the left, requiring a positive yaw moment (nose-right) to restore its trim condition (21).

$$C_{n_\beta} = \frac{\delta N}{qS_v b \delta\beta} \tag{2–7}$$

Finally, the roll stability coefficient, C_{l_β}, is the derivative of the roll moment with respect to the angle of sideslip. This derivative must be negative to be stabilizing. If a positive sideslip angle causes the plane to roll its right wing down, then a positive sideslip angle will be induced, creating instability. Instead, geometry of the aircraft needs to roll the plane's left wing down. This effect is produced partially by the vertical tail. A vertical tail above the center of gravity would produce a negative roll in the presence of positive sideslip. The wing geometry can also contribute to the stabilizing effect by creating a higher local angle of attack on the right wing, hence, greater lift on that wing. The lift differential produces a negative rolling moment, pointing the left wing down. As the plane rolls, the sideslip is reduced (21), (19).

$$C_{l_\beta} = \frac{\delta L}{qS_w b \delta\beta} \tag{2–8}$$

2.5 Rotation Damping

Aircraft have three rotation damping derivatives that serve to oppose rotations caused by the stability coefficients above.

The first is the production of pitch moment by an incremental pitch rate, C_{m_q}, and is largely ignored by this thesis. This derivative is affected predominantly by the horizontal

tail. A larger tail placed further from the center of mass along the longitudinal axis produces a larger pitch damping effect (21).

$$C_{m_q} = \frac{\delta C_m}{\delta q} \tag{2–9}$$

The second is the production of roll moment by an incremental roll rate, C_{l_p}. This derivative is affected by the size and span of wings, horizontal tail, and vertical tail. Any increase in the size or span of these surfaces increases the roll damping derivative (21).

$$C_{l_p} = \frac{\delta C_l}{\delta p} \tag{2–10}$$

Finally, C_{n_r} is the increase in yaw moment from an increase in yaw rate. The vertical tail's size and separation from the center of mass along the longitudinal axis are the most important variables to C_{n_r}. An increase in either of those variables would increase the yaw damping derivative (21).

$$C_{n_r} = \frac{\delta C_n}{\delta r} \tag{2–11}$$

2.6 Control Effectiveness

Control effectiveness derivatives are non-dimensional measurements of the efficiency with which a deflection of one of the control surfaces can produce a net force or moment on the aircraft. There are many of these derivatives that relate deflections of any of the three control surfaces to any of the six forces or moments on the aircraft. Many of these will be dismissed in this thesis due to being negligible when compared to other control surfaces designed to be the primary control effector for a given force or moment.

The control effectiveness coefficients relevant to this thesis are given in Equations 2–12 - 2–18 (21).

- Lift with respect to elevator deflection

$$C_{L_{\delta elev}} = \frac{\partial C_L}{\partial elev} \tag{2–12}$$

- Lift with respect to aileron deflection

$$C_{L_{\delta ail}} = \frac{\partial C_L}{\partial ail} \tag{2–13}$$

- Pitch moment with respect to elevator deflection

$$C_{m_{\delta elev}} = \frac{\partial C_m}{\partial elev} \tag{2–14}$$

- Roll moment with respect to aileron deflection

$$C_{l_{\delta ail}} = \frac{\partial C_l}{\partial ail} \tag{2–15}$$

- Roll Moment with respect to rudder deflection

$$C_{l_{\delta rudd}} = \frac{\partial C_l}{\partial rudd} \tag{2–16}$$

- Yaw moment with respect to aileron deflection

$$C_{n_{\delta ail}} = \frac{\partial C_n}{\partial ail} \tag{2–17}$$

- Yaw moment with respect to rudder deflection

$$C_{n_{\delta rudd}} = \frac{\partial C_n}{\partial rudd} \tag{2–18}$$

2.7 Flight Performance Equations

In steady level flight the aircraft experiences no accelerations along or about any axis. Thus, all moments and rotation rates must be zero, and the forces on the aircraft must be equal and opposite (20).

$$\begin{aligned} T = D = qSC_D \\ where, \\ T = thrust \\ D = drag \\ C_D = drag\ coefficient \end{aligned} \tag{2–19}$$

$$W = L = qSC_L$$

$$where,$$

$$W = weight \tag{2–20}$$

$$L = lift$$

$$C_L = lift\ coefficient$$

In level turning flight, the aircraft is banked so that the lift vector provides the force required to turn. The forces must change to maintain force balance in the vertical direction (20).

$$W = L\cos\phi = qSC_L\cos\phi$$

$$where, \tag{2–21}$$

$$\phi = bank\ angle$$

The resultant force on the aircraft becomes a function of the weight of the vehicle and its load factor (20).

$$F_r = \sqrt{L^2 - W^2} = W\sqrt{n^2 - 1}$$

$$where, \tag{2–22}$$

$$n = load\ factor = \frac{L}{W} = \frac{1}{\cos\phi}$$

According to Newton's second law, the radial acceleration of an object is a function of its velocity and the radius of curvature of its path (20).

$$a_{rad} = \frac{V_\infty^2}{R}$$

$$where, \tag{2–23}$$

$$V = velocity$$

$$R = turn\ radius$$

So, the resultant force must create this acceleration. Equating the resultant force to the inertial force created by the centripetal acceleration (20).

$$\frac{W}{g}\frac{V_\infty^2}{R} = W\sqrt{n^2-1}$$

$$where, \tag{2–24}$$

$$g = gravitational\ constant$$

This equation can be solved for either turning radius, R, or angular velocity, ω, yielding the equations below (20).

$$R = \frac{V_\infty^2}{g\sqrt{n^2-1}} \tag{2–25}$$

$$\omega = \frac{g(n-1)}{V_\infty} \tag{2–26}$$

Note that only two variables impact the turning performance of the aircraft, the velocity at which the vehicle is traveling and its load factor. Recall from Equation 2–22 that load factor is just a function of the bank angle. Thus, it is concluded that to improve turn performance, ie. reduce turn radius and increase turn rate, then its velocity should be reduced and bank angle should be increased.

2.8 Aerodynamics Prediction

The research uses a standard aerodynamics prediction code to analyze the trimmed flight conditions and dynamics of flight vehicle models. The code used is called Athena Vortex Lattice (AVL) and is written by Mark Drela and Harold Youngren of the Massachusetts Institute of Technology. This research uses AVL version 3.26.

A vortex lattice method of aerodynamics prediction first divides the lifting surfaces and bodies into small surfaces. Then, by modeling the path of vortices off of the model, the code calculates the flow velocity orthogonal and parallel to each incremental surface area. The flow velocities are then converted into normal and shear forces on that section of the body. Finally, the forces are compiled to find the total forces and moments on the entire model.

AVL has the ability to find a trim condition subject to user-input constraints on the aircraft's flight variables. Once the trim condition is found and all forces and moments are compiled, AVL proceeds to calculate the linearized dynamics of the model. These dynamics can be output as either the stability derivatives explained above, or as the full 12-state dynamics matrices.

2.9 Turn Performance Evaluation

There is a need for a normalization constant to evaluate turning performance metrics. AVL does not permit bank angle to vary to find a trim condition; instead, other parameters are forced to adjust to trim at the specified bank angle. For this reason, the bank angle is held constant when analyzing turn performance. Consequently, the configurations could not be tested at a constant velocity, or else all of their turn performance metrics would be identical. To analyze the performance, another metric had to be held constant.

The physical limitation of the power plant supplying thrust for the vehicle is chosen to be that metric. By testing cases at varying velocities, the research uncovered the intersection between the required plant output in the test case matrix and the vehicle's limits. However, there are two methods to constrain the output of the plant: constant available thrust or constant available power. Thrust must be equal to drag at trimmed flight conditions; so, the limits placed on the vehicle are equivalent to constant required thrust (equivalent to constant drag) and constant required power (equal to a constant product of drag and velocity) (20).

A constant available thrust model is a standard assumption for jet aircraft, whereas a constant available power model is typically applied to propeller-powered aircraft and biological organisms. Simply put, a jet engine can produce the same thrust force at all velocities, while a propeller engine or animal can produce greater forces at lower speeds than at higher speeds (20).

In this thesis, an aircraft model's turn performance is normalized with respect to both constant thrust and constant power models to fully demonstrate its turn performance. A biological system's turn performance is normalized with respect to constant thrust rather than constant power because of the assumptions made in the model. The organism in question is assumed to be in gliding flight rather than flapping flight; thus, no power is imparted to the oncoming airflow. In gliding flight, the most important metric is lift to drag ratio, because this ratio determines the flight endurance and range. Lift is held constant through all test cases to hold the vehicle in level flight, so the drag is the important characteristic to normalize.

2.10 Eigenvector Analysis

Any square nxn matrix of full rank, A, has n distinct eigenvalues, λ, and eigenvectors, v, that satisfy Equation 2–27 (22).

$$Av = \lambda v \tag{2–27}$$

If the matrix, A, represents the linearized dynamics of a system about an equilibrium point, then its eigenvalues and eigenvectors tell a great deal about the system's modes. Each eigenvalue-eigenvector pair represents the dynamics of one mode.

The eigenvalue (also called the mode's time constant) tells whether the mode is oscillatory or not, and how quickly the system will converge back to steady-state conditions or diverge away from steady-state conditions. A negative eigenvalue is stable and will return the system to its equilibrium, while a positive eigenvalue will drive the system away. Imaginary eigenvalues indicate oscillatory motion.

The relative magnitudes of the components of the eigenvector tell how much each state is affected by the mode and whether the states are in or out of phase. Larger eigenvector components indicate a greater effect on that state.

CHAPTER 3
BIOLOGICAL INSPIRATION

3.1 History

Pterosaurs were a branch of archosaurs that achieved large-scale powered flight before any other animals. Only birds, bats, and insects have been able to duplicate this feat of evolving independent methods for powered flight by flapping. Each group has acquired different styles of flight because of different body plans and environmental conditions. Pterosaurs were the first vertebrates that took to the air around 225 million years ago, at about the same time dinosaurs first spread across the continents. Both birds and pterosaurs evolved in the Mesozoic, whereas bats evolved in the early Tertiary soon after the demise of pterosaurs. Insects will largely be excluded from discussion because although they have evolved powered flight, they operate at scales in which the different fluid mechanics phenomena dominate, making it difficult to envision an insect modeled system capable of carrying payloads on the same scale as current common sensing equipment. Pterosaurs first appeared in the fossil record during the late Triassic, diversified into an extraordinary variety of forms and sizes during the Jurassic and Cretaceous periods, and dominated the Mesozoic sky for 160 million years above the heads of dinosaurs. They became extinct at the end of the Cretaceous period, about 65 million years ago, along with the dinosaurs (18).

3.2 Pterosaur Anatomy as a Model for Aircraft Design

Pterosaurs are remarkably suitable for biologically-inspired design of aircraft. The community has invested considerable effort into the study of birds and insects for design; however, pterosaurs are actually very appropriate for a variety of reasons.

Pterosaurs succeeded in a great variety of size ranges and modes of flight. Pterosaurs thrived for 160 million years until the sudden biological catastrophe that drove much of the globe's species to extinction. During their time, pterosaurs evolved into a great range of diverse organisms. Wingspans ranged from 0.4m to 10.4m. Similarly, body masses

reached values as low as 15 grams and as high as 70 kg. Not only did pterosaurs vary greatly in size, but also in their methods of locomotion. Chatterjee and Templin studied the flight performance of pterosaurs using a computer simulation model and recognized three different styles of flight. Smaller pterosaurs (Mass 0.01-0.2 kg) were capable of hovering flight, much like hummingbirds of today. The medium-sized animals (Mass 0.3-9.0 kg) were capable of powered flight, comparable to birds of the same size. The largest pterodactyloids such as Quetzalcoatlas became the largest aerial animals that ever flew. These enormous creatures (Mass 10 - 70 kg) probably adopted soaring flight, using flapping minimally, and preferring to use columns of warm, rising air to gain sufficient lift (18).

The environment that pterosaurs inhabited forced them to overcome many of the challenges that engineers face when trying to design a MAV capable of urban surveillance. Many small to medium sized pterosaurs lived in the forests, so they must have been capable of sophisticated obstacle avoidance. Medium to large sized pterosaurs stayed predominantly near the coast, living like common day pelicans and using the high winds to gain sufficient lift: so, these pterosaurs must have been able to maintain stability in windy conditions (18).

Pterosaur anatomy is uniquely unlike that of bats and birds and remarkably similar to the structure commonly used in modern MAV's. Pterosaurs used a leading edge spar to support a membrane that serves as the lifting surface. This membrane was also stiffened by a densely spaced set of fibers called actinofibrils. These fibers acted much like the carbon fiber used to support the lifting membrane on MAV's, transporting the stresses to the leading edge spar, preventing extreme airfoil shape change, and reducing the likelihood of catastrophic damage to the wing membrane (18).

A further comparison between biological and mechanical flight systems is shown below to demonstrate the aptitude for modeling a small MAV design on pterosaurs.

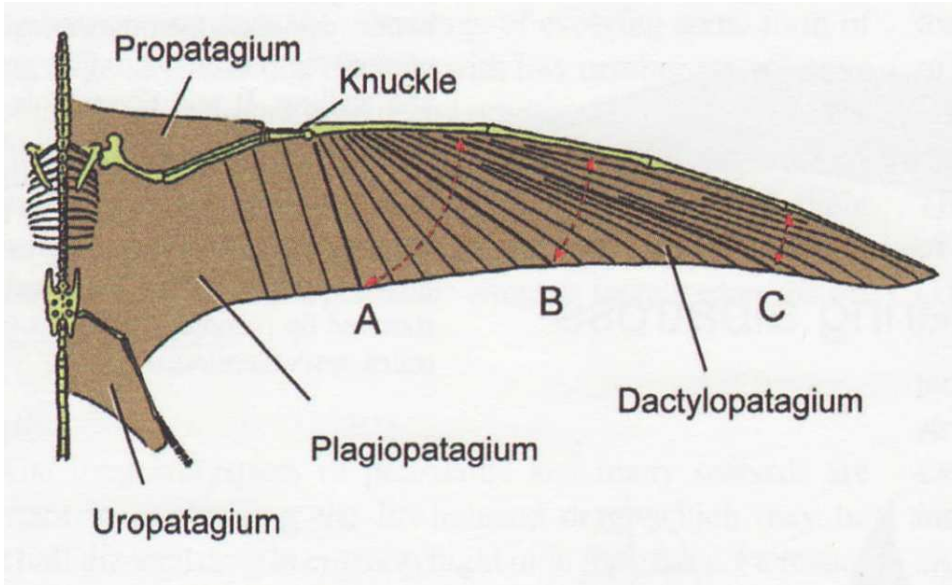

Figure 3-1. Image of Pterosaur Actinofibrils

platform	wing surface	muscle actuation	flapping motion	vertical tail	wing extenders	structural elements
insect	rigid	low	high	no	no	chord-span
bird	feather	high	high	no	feathers	span
bat	membrane	high	high	no	joints	chord-span
pterosaur	membrane	low	low	yes	joints	span
MAV	membrane	low	low	yes	joints	span

Table 3-1. Properties of Flight Platforms

Pterosaurs are of particular interest due to the ability to both walk on the ground and sail over water in addition to flight. Such multi-modal locomotion enables an incalculable range of missions. An aircraft based on pterosaur concepts may be able to fly to a rooftop then walk under an overhang to mount a sensor in a dark corner. Additionally, their quadrupedal gait is much simpler to manufacture and control than the bipedal gait that birds and bats commonly employ.

So, pterosaurs have a proven track record of aerodynamic success and due to their anatomy and methods of locomotion, serve as a sensible model around which to base a multi-locomotive sensory system capable of navigating dense obstacle fields and efficiently sensing their environment.

3.3 Cranial Crest

However, pterosaurs have a particularly interesting aerodynamic feature that has not been characterized before. The large cranial crest on their heads is seen below. While its relative size varied between species and its full purpose is still debated, its aerodynamic impact is unavoidable. In some way this crest must have acted like a vertical tail. The difference is its placement in front of the center of gravity of the pterosaur. Common sense would dictate that such a placement would create large instabilities, as a wind gust from the right would yaw the pterosaur left, thus creating an even larger wind force acting to yaw the pterosaur further. This expectation begs the questions, how did the pterosaurs compensate for the creation of this lateral instability and was there any aerodynamic advantage to placing this aerodynamic surface in front of the center of gravity to justify the instability created?

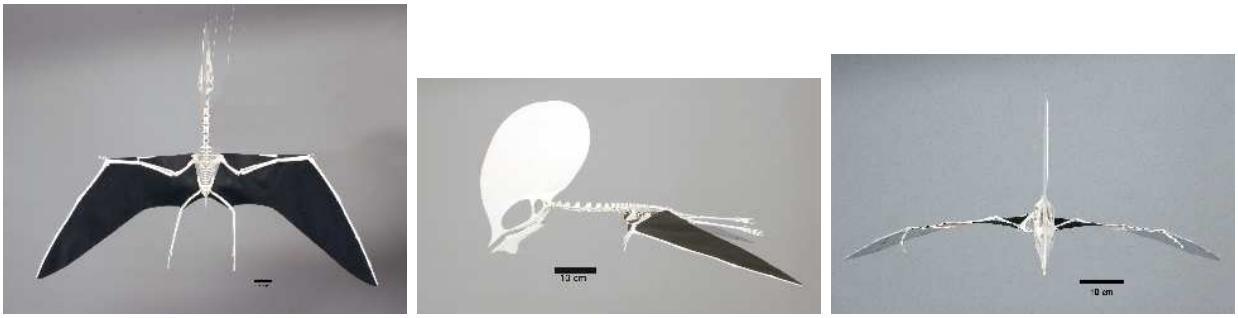

Figure 3-2. Skeletal Reconstruction of an Early Cretaceous Pterosaur, *Tapejara wellnhoferi*

An evolutionary perspective would suggest that the benefits must have at least compensated for the stability losses. So, the research focused on the pterosaurs that lived near the coasts. These animals needed to be able to takeoff from either a cliff's edge or the shore, control their flight in a turbulent atmosphere, maintain a desired flight path and flight dynamics while turning their head to observe predators or prey, and then land safely. A pterosaur's daily survival depended on a very similar mission profile to the one described in the introduction, making these pterosaurs an ideal candidate for research into how biological systems could be adapted for MAV research.

3.4 Chosen Species

The researcher selects the *Tapejara wellnhoferi* to be the species to model. This species is chosen for both its mission characteristics and its size and control actuation capabilities. Previous studies in the researcher's lab studied morphing effects in MAV's with a wingspan of roughly one meter (7),(5). *Tapejara* had a wingspan of 1.35 meters and had several joints along its wing that permitted rotation in the coronal plane (18). The result of joint rotations along *Tapejara*'s wing is a leading edge wing sweep change at discrete locations along the spanwise axis, which is exactly the effect produced by previous research by Grant (7). This similarity allowed the researchers to examine the interaction between the forward placed vertical tail and wing sweep morphing.

This particular species also had an unusually large crest, making the aerodynamic effects due to the presence of that surface more dominant and easier to identify. Additionally, a nearly complete and three-dimensional skeleton of *Tapejara* was found in the Santana Formation in Brazil with a soft tissue crest on the head. This unique discovery increases the knowledge base of the biological system so that the dynamics and potential movements can be modeled with greater fidelity.

CHAPTER 4
PTEROSAUR FLIGHT ANALYSIS

4.1 Pterosaur Model

Every effort is made to make a computer model of *Tapejara* that matches the information available from fossil records.

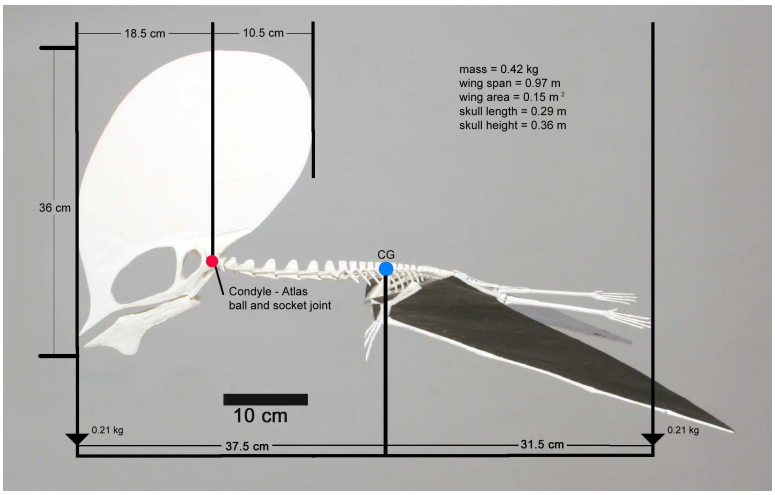

Figure 4-1. Image of Measured *Tapejara* Skeletal Reconstruction

4.1.1 Aerodynamic Geometry

The first step in modeling *Tapejara* is the geometric definition of the nominal configuration. The wings are defined using leading and trailing edge points that are obtained from scale models reconstructed from casts of *Tapejara*'s skeleton. These leading and trailing edge coordinates are defined at 71 points along *Tapejara*'s wingspan. The wings are also given an airfoil shape that is obtained from previous pterosaur research (18). The head is also modeled using the geometry of a skeletal cast by 16 sets of coordinates, spaced evenly along the vertical direction. These parts of *Tapejara* are modeled as infinitely thin lifting surfaces, which is justifiable because of the nature of the membrane structure of the pterosaur's wing.

The other parts of *Tapejara* are modeled as cylindrical bodies. So, the neck is defined as a constant diameter cylinder extending from the front of the torso into the middle of the head to include the effects of the thickness of the head that exceeds negligible limits. The legs are modeled as two separate constant thickness cylinders extending from the hip joint on the back of the torso. The hip joint is located using skeletal reconstructions. The torso is modeled as a cylindrical body with both a diameter and centerline that are variable so that the model can capture both the lengthwise changes in thickness of the torso and its relatively flat dorsal surface.

The resulting geometric model is shown below.

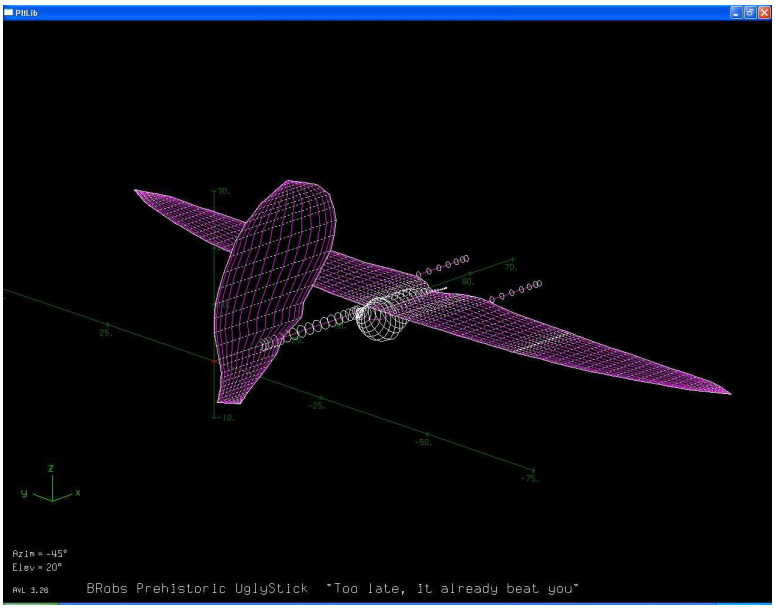

Figure 4-2. Isometric View of *Tapejara* Model in Nominal Wing Position

4.1.2 Masses and Inertias

The model is divided into its body parts to more accurately model the mass distribution of *Tapejara*. The head, inboard wing sections, and outboard wing sections are modeled as trapezoidal prisms of constant thickness and density. The neck, torso, and legs are modeled as cylinders of constant density. The volumes are then integrated to find the centers of mass and moments of inertia. The resulting data are shown in the table below:

Body Part	Mass (g)	I_{xx} (gcm^2)	I_{yy} (gcm^2)	I_{zz} (gcm^2)	I_{xy} (gcm^2)	I_{xz} (gcm^2)	I_{yz} (gcm^2)
Torso	200	1600	2467	2467	0	0	0
Head	120	18542	43192	24730	0	17202	0
Neck	20	40	260	260	0	0	0
Left Inboard Wing	20	1347	518	1861	-195	0	0
Right Inboard Wing	20	1347	518	1861	195	0	0
Left Outboard Wing	10	2268	629	2896	116	0	0
Right Outboard Wing	10	2268	629	2896	-116	0	0
Left Leg	10	1.25	1.25	334	0	0	0
Right Leg	10	1.25	1.25	334	0	0	0

Table 4-1. Masses and Inertias of Modeled Parts of *Tapejara*

The body parts are treated as point masses to find the model's center of mass, but use the given moments of inertia to capture its dynamics.

4.1.3 Wing Control Effectors

The methods by which *Tapejara* controls its flight need to be modeled to capture its flight characteristics. Pterosaurs had an anatomy that did not permit the highly refined wing morphing, such as radical changes in wing twist or camber distributions, seen in other flying animals. Pterosaurs had muscles that allowed for a relatively constant wing twist, but the lack of pronounced musculature in its membrane wing structure and the stiff actinofibrils prevented more articulated control actuation. So, the model can vary the total wing twist either symmetrically to act as an elevator, or asymmetrically to act as a set of ailerons. The span of each wing from the bone at the leading edge to the trailing edge is combined with the propatagium flap to be defined as the elevator. The same region is also defined as the aileron because *Tapejara* could twist its right and left wings independently. These control surface definitions allow the model to be able to achieve any combination of right and left wing twist, using simultaneous symmetric (elevator) and asymmetric (aileron) twist.

4.1.4 Morphing

Tapejara also had the ability to alter its wing configuration by folding at its joints. To model the changes, the coordinates for the wing's skeletal elements are recorded at their fully extended positions and then their rotated positions are found after the joints are folded. *Tapejara* had joints at the shoulder, elbow, wrist, and first knuckle joint (the other knuckle joints are fused together). The limb joints of the Cretaceous pterosaur *Tapejara wellnhoferi*, as shown in Figure 4-3, are analyzed to estimate the range of movement during terrestrial and aerial locomotion.

The shoulder joint had a vertical range of motion of 85°, used for flapping the wing, and can be folded backwards from a fully extended longitudinal position to within 25° of its anteroposterior axis. The model assumes this joint to be fixed in its fully extended horizontal position because the model intends to analyze gliding rather than powered

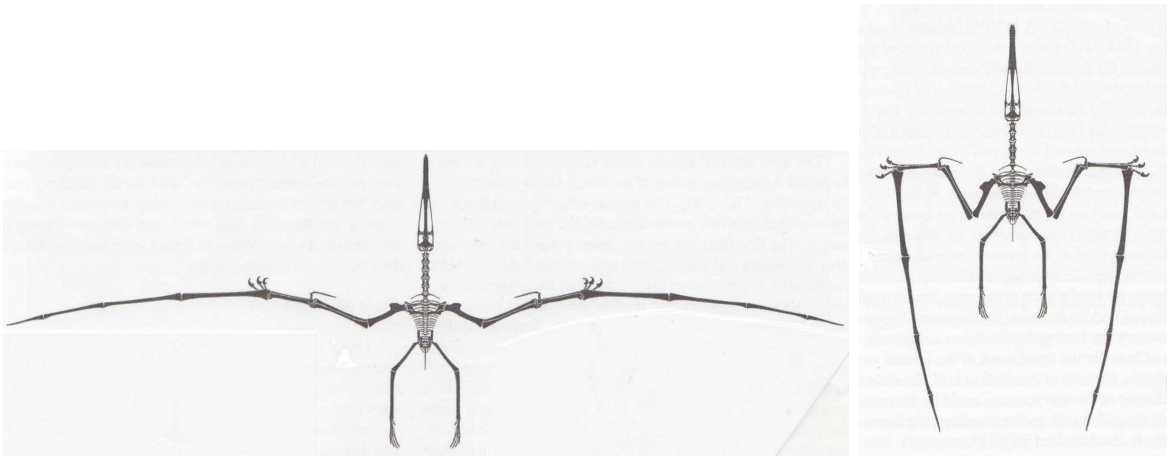

Figure 4-3. Top View of *Tapejara* Skeleton in Extended and Folded Wing Positions

flight, and because folding the wing towards the body at the shoulder joint collapses the entire wing to the body to assist in walking.

The elbow joint's nominal position put the radius and ulna of *Tapejara*'s wing at a 145° angle to the humerus and could sweep forward to make a 90° angle to the humerus. The model allows the elbow joint 30° of its full 55° range of motion. The range of motion is constrained because the extreme joint angles drastically reduce the wing area, making flight at such configurations unlikely.

The wrist joint had the smallest range of motion of any of the joints, allowing only 30° of sweep backward from its nominal position. The wrist joint was held fixed in the model because it has such a small range of motion and is close to the knuckle joint, which produces a nearly identical effect on a larger scale.

The knuckle joint was held at a 165° angle in *Tapejara*'s nominal position and could fold backward to form an angle as small as 35°. The model allows a range of motion of only 65° because once the knuckle joint is folded that close to the body, the outboard wing area becomes negligible, so further rotation at that joint would have little effect.

The research is made tractable by fixing the shoulder and wrist joints at their extended positions, and by allowing the knuckle and elbow joints a limited range of motion, the model still allows both sweep in the fore and aft directions to capture

trends in the trimmed flight dynamics. A tabular summary of *Tapejara*'s wing morphing capabilities and the investigated range is shown in Table 4-2, and some images of a sampling of morphed models are shown in Figure 4-4.

Joint	Sweep Direction	True Range of Motion	Tested Range of Motion
Shoulder	Backward	55°	fixed
Elbow	Forward	55°	30°
Wrist	Backward	30°	fixed
Knuckle	Backward	130°	65°

Table 4-2. Joint Range of Motion

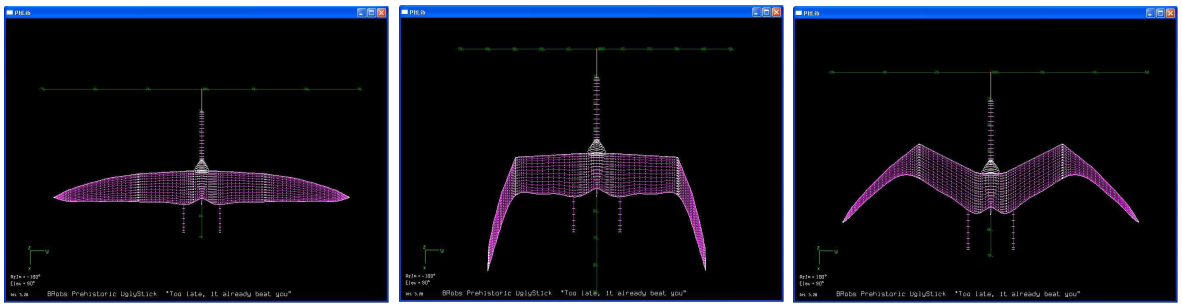

Figure 4-4. Top View of Model in Various Morphed Wing Positions

Figure 4-5 shows how morphing at the knuckle joint is complicated by the fact that deflection causes the wing to begin to fold into itself, thus reducing the surface area of the outboard section of the wing. So, some of the actinofibrils are modeled as they rotate with the wing, providing coordinates for the rotated leading and trailing edge coordinates. The angles between the actinofibrils are assumed to decrease proportionately to the angle of knuckle rotation until they completely fold together at an angle 10° past the posterior axis. Justification for these limits comes from diagrams of folded pterosaur wings (18).

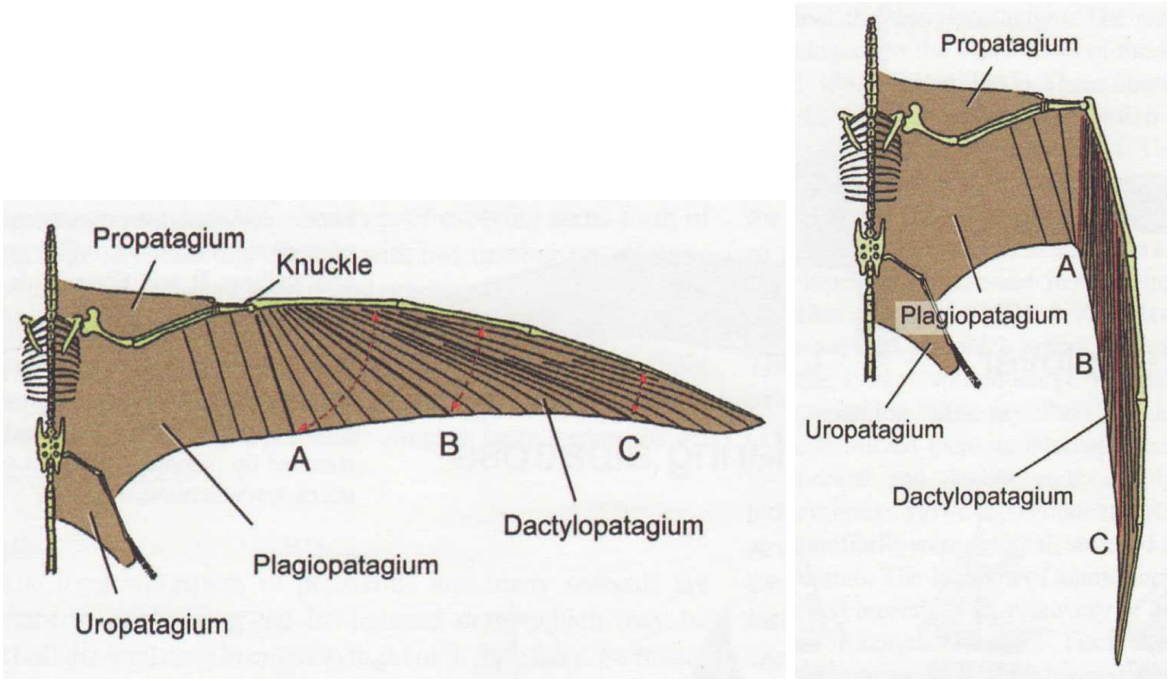

Figure 4-5. Top View of *Tapejara* Pterosaur Wing in Extended and Folded Wing Positions

4.1.5 Cranial Movement

Tapejara could also move its head about a ball and socket joint at the base of its head, thus allowing three degrees of freedom through which it can rotate. Rotations about the left-right and anteroposterior axes are ignored because those rotations have minimal direct effect on the flow past the head. Rotation about the dorsoventral axis severely disrupts the flow past the head and would be the most effective use of the head as a control surface. So, rotations of the head are modeled as rotations about the vertical axis through the head at the Condyle-Atlas joint. Combined rotations about the anteroposterior and dorsoventral axes could combine for some interesting effects on both yaw and pitching moments, but these possibilities are not investigated to keep the degrees of freedom of the model down to a manageable level (18).

4.1.6 Model Summary

In summary, the model is designed to simplify *Tapejara*'s dynamics to a tractable research problem while still sufficiently capturing its aerodynamic and inertial phenomena. The model possesses 7 independent control methods, of which some have analogous parts in aircraft design: head rotation (hereafter referred to as rudder deflection), symmetric wing twist (elevator deflection), asymmetric wing twist (aileron deflection), forward sweep at each elbow joint, and backward sweep at each knuckle joint. The wing sweeps are used as independent variables set by the researchers. The head rotation and wing twists are primarily used as the dependent variables, allowing them to adjust to find *Tapejara*'s trimmed flight condition.

4.2 Steady Level Flight Analysis

4.2.1 Run Conditions

The pterosaur model is tested in steady, level flight to investigate the trimmed flight conditions that the pterosaur used, and the stability characteristics of those flight configurations. The model is analyzed at varying deflection angles of its head and for

varying joint angles along the wing. The wing joints are altered both symmetrically and asymmetrically.

During the symmetric sweep runs, the elbow and knuckle joint angles are morphed through the model's range of motion with the left and right wings remaining identical. As a result, the most dominant trends are changes in the longitudinal flight conditions, with some accompanying effects seen in the lateral and longitudinal dynamics.

Asymmetric sweeps are conducted by flexing the left elbow and the right knuckle through the same positions used in the symmetric configurations. These combinations of morphing are conducted to attempt to capture the most extreme yawing and rolling effects, thus showing the conditions through which *Tapejara* could maintain steady, level flight.

All test runs are done at a velocity of 10 m/s. This velocity is chosen because it is near the cruising speed of *Tapejara* of 8 m/s (18). However, AVL encounters difficulties finding trim conditions for the model at velocities below 9 m/s. Consistent with the steady, level trimmed flight definition, the bank angle and all rotational rates and moments are forced to zero. The wing control surfaces are allowed to rotate to balance pitching and rolling moments, while the angle of attack is constrained to provide sufficient lift for the model to maintain level flight.

In some cases, the head control deflection angle is allowed to vary to maintain a constant sideslip angle of zero. In these tests the head is essentially acting as a rudder to balance moment while maintaining a desired aircraft body condition, so it is referred to as rudder angle in the plots. In other cases the head control deflection angle is forced to zero, so that the head will not be permitted by AVL to rotate to balance the yawing moment. These cases are referred to as head-fixed analysis. It is necessary to examine this condition because holding the head fixed is an important biological configuration. *Tapejara* needed to have the freedom to point its vision in the direction of prey, a possible nesting site, or any other region of interest. This need created what is essentially a sensor pointing

problem for *Tapejara*. So, while the wings are swept asymmetrically, the head is held to a constant angle of 10°, and the sideslip angle (the angle with respect to the oncoming airflow in the coronal plane) is allowed to be nonzero to balance out the moments.

4.2.2 Symmetric Sweep Results

4.2.2.1 Trimmed Flight Conditions

As the elbow joint angle is increased or the knuckle joint angle is decreased the wing area is moved further forward along the anteroposterior axis. Thus, the lifting force moves in the same direction, moving closer towards the center of mass of *Tapejara*. Moving the center of the lifting force reduces the moment that must be produced by the wings to counteract the torque created by the distance between the center of mass and the center of lift. Consequently, less wing twist is required, allowing *Tapejara* to fly at lower angles of attack, while still producing the necessary amount of lift. Flight at lower angles of attack and with less wing twist results in a smaller drag coefficient. So, sweeping the wing forward at the elbow and keeping the knuckle joint as small as possible results in a lower drag coefficient.

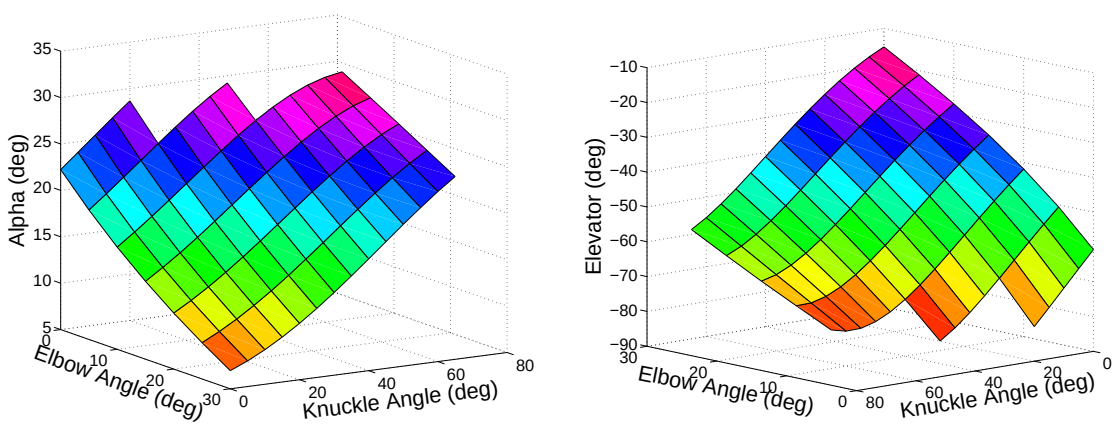

Figure 4-6. Angle of Attack and Elevator Deflection in Steady Level Flight

However, increasing the knuckle joint angle also decreases the wing area so that any increases in drag coefficient are offset and the resulting drag decreases. So, sweeping the

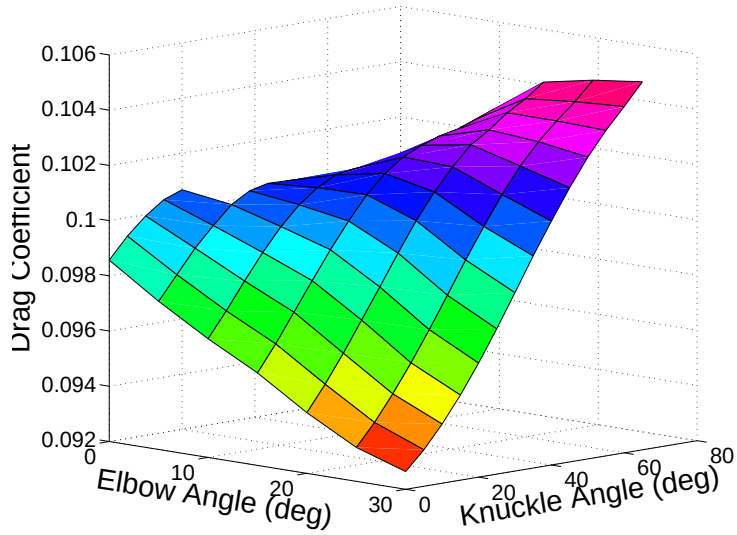

Figure 4-7. Drag Coefficient in Steady Level Flight

wing forward at the elbow and back at the knuckle would have allowed *Tapejara* to fly with the least total drag.

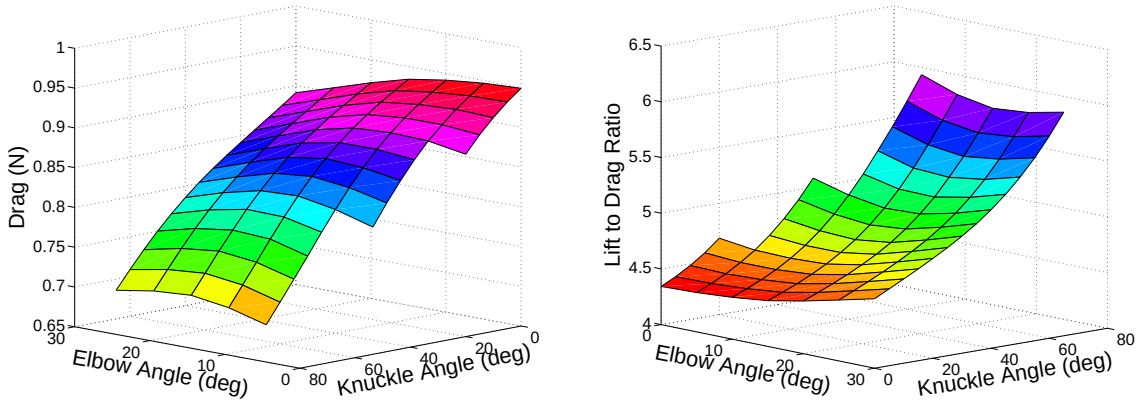

Figure 4-8. Drag and Lift-to-Drag Ratio in Steady Level Flight

This result shows that *Tapejara* likely used wing morphing to alter its trim flight condition to be more efficient. So when high velocity flight is necessary, *Tapejara* could morph its wings into a configuration that would produce less drag.

4.2.2.2 Static Stability

The static stability coefficients are found at each trim condition. Recall that a positive C_{n_β} is stable and that a forward placed vertical control surface is destabilizing with respect to a sideslip. Thus, the negative C_{n_β} values are to be expected. The model's yaw stability coefficient increases as the wings are swept forward at the elbow, while flexion at the knuckle joint has a similar, but much less pronounced effect. *Tapejara*'s roll stability coefficient decreases with sweep back at the knuckle joint, but increases as the elbow sweeps the wings forward. This effect occurs because the wing surface becomes less efficient, allowing the rudder to stabilize *Tapejara* in the roll axis with respect to sidewinds.

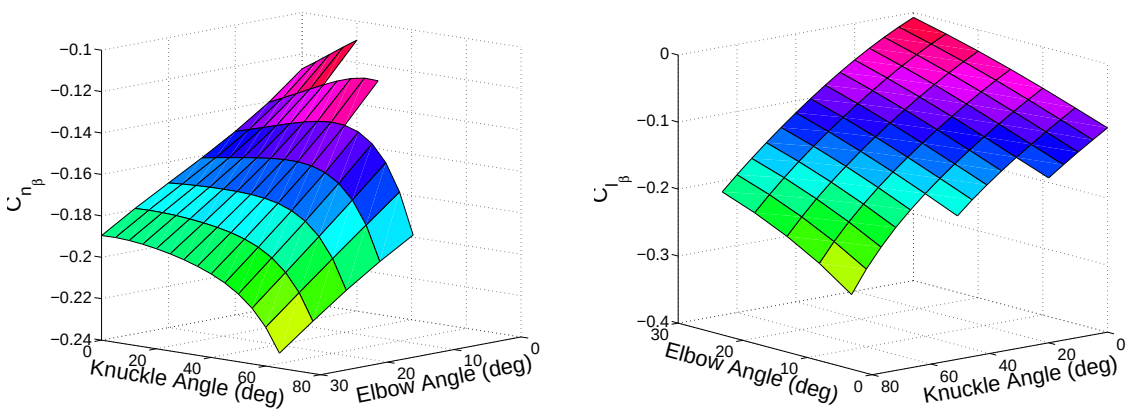

Figure 4-9. Yaw and Roll Stability in Steady Level Flight

The wings are far less effective at producing lift when the wings are swept backward at the knuckle joint, but improve their effectiveness when they sweep forward at the elbow joint. This trend is consistent with performance improvements seen in forward-swept wing aircraft (20). The longitudinal static stability coefficient increases with elbow sweep forward and increases with sweep backward at the knuckle joint. So, the effect shows consistently that as the wing area is pushed further aft the distance between the center of lift and the center of mass increases, making the aircraft more pitch stable.

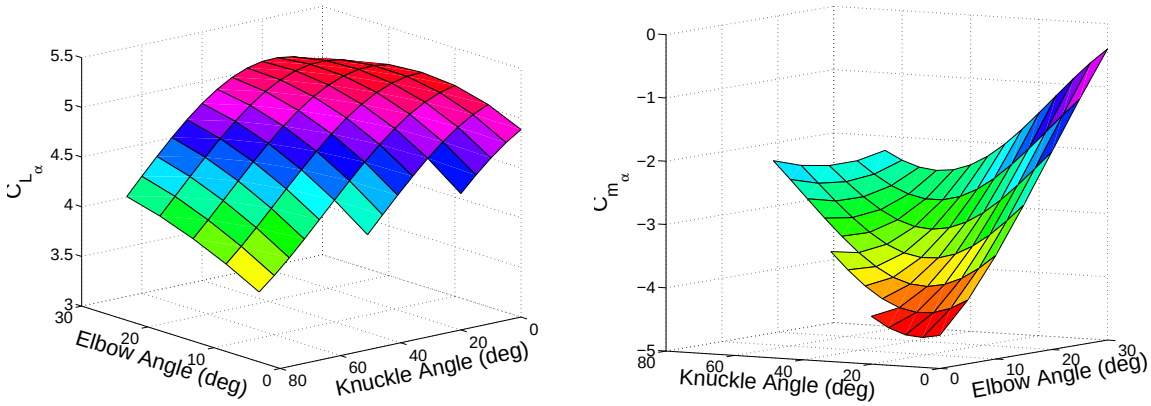

Figure 4-10. Lift Slope and Pitch Stability in Steady Level Flight

4.2.2.3 Rotation Damping

The roll and yaw damping data also show that the rudder becomes the more dominant control surface when wing sweep morphing occurs. As the wing is folded at the knuckle joint, the amount of wing area far from the anteroposterior axis is reduced, thereby decreasing the amount of wing area that acts to damp out roll rates, decreasing C_{l_p}. Roll damping increases in magnitude slightly with elbow flexion, probably because the nominal wing shape is slightly swept back, so forward sweep would increase the moment arm of the wing area with respect to roll moments. An increase in the magnitude of the yaw damping coefficient, C_{n_r}, accompanies flexion at both wing joints. As the wing joints flex, the wings' moment arm with respect to yaw moment decreases, making the rudder's effect on the flight dynamics more pronounced with respect to yaw moment; thus, causing the yaw damping coefficient to increase by 230%.

4.2.2.4 Control Effectiveness

The wing becomes tucked in closer to the body as the wing is morphed at the elbow, reducing the yaw moments that a drag force on the wing would create. As the wing is morphed at the knuckle, the area of the wing furthest from the dorsoventral axis is severely reduced, thus reducing the yaw moments the wing could create. These two effects dominate the trends seen in the stability and control coefficients. As the elbow

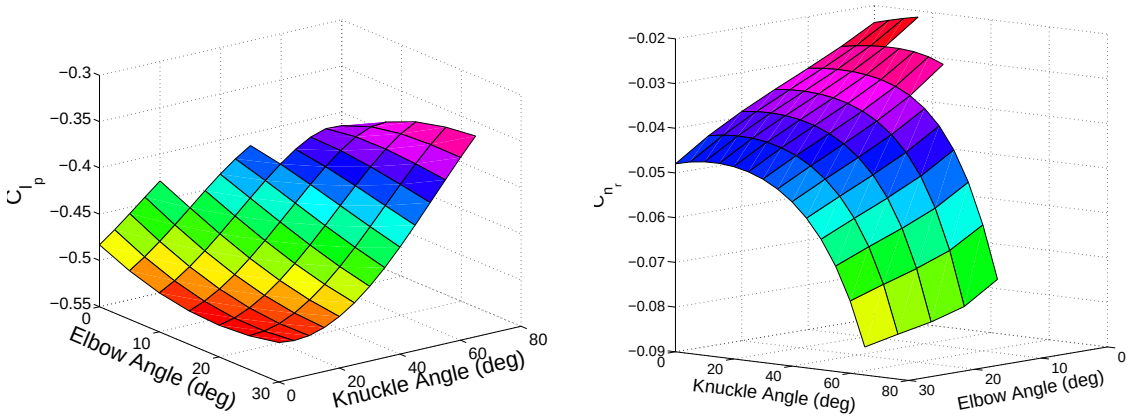

Figure 4-11. Roll and Yaw Damping in Steady Level Flight

and knuckle joints are flexed, the yaw moments become dominated by the actions of the head. C_{n_β} becomes increasingly negative with morphing at both joints, showing that the destabilizing effect of the head in front of the center of mass is becoming even more dominant.

The control coefficient $C_{n_{\delta ail}}$ decreases with increasing flexion at each joint, while $C_{n_{\delta_r udd}}$ increases, showing that morphing decreases the effect that the wings have on yawing *Tapejara* and increases the effect that the head has on yaw.

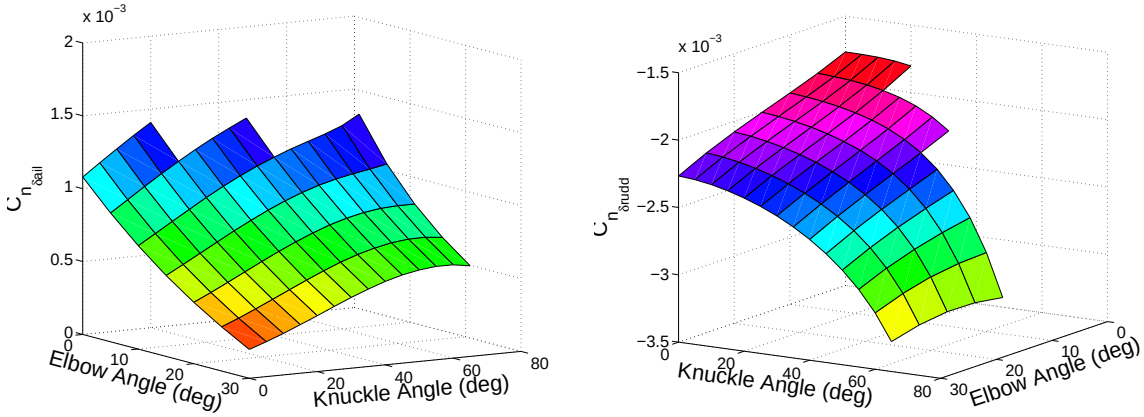

Figure 4-12. Yaw Effectiveness of Ailerons and Rudder in Steady Level Flight

This trend indicates that as the wing is morphed (either forward at the elbow joint or backward at the knuckle joint) the head becomes a more dominant control surface,

because its effectiveness on influencing yaw moments increases. Thus, the coupling between the effects of wing sweep morphing and the aerodynamic effects of having a large forward-placed vertical tail is of vital importance, and the presence of both in *Tapejara* makes it an interesting aerodynamics example.

As the knuckle joint is flexed, the same effects are seen with respect to roll moments. An increase in knuckle flexion reduces the wing area furthest from the anteroposterior axis, thus reducing the wing's control over roll. C_{l_β} increases, $C_{l_{\delta ail}}$ decreases, and $C_{l_{\delta rudd}}$ increases as the knuckle sweeps back. However, as the elbow joint is flexed, the wing's effect on roll is increased.

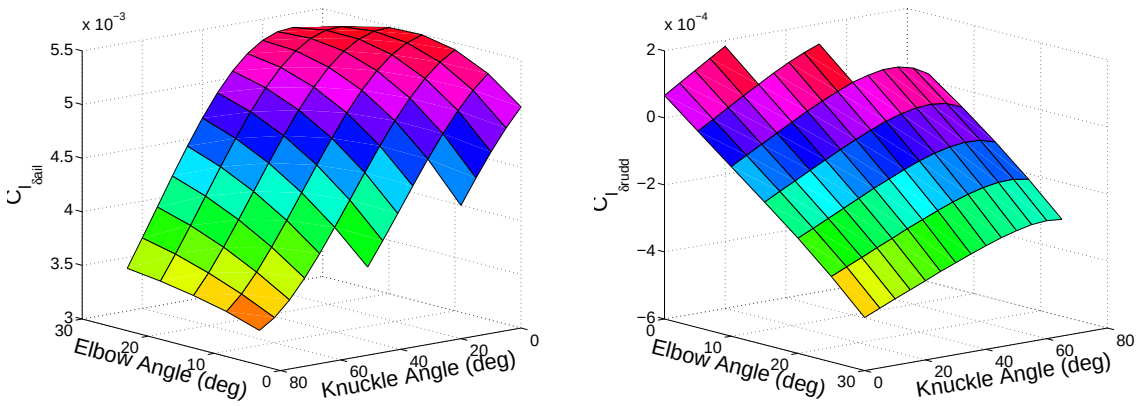

Figure 4-13. Roll Effectiveness of Ailerons and Rudder in Steady Level Flight

$C_{m_{\delta elev}}$ decreases as the elbow is flexed because the wing's distance from the left-right axis is decreasing. This change is much more prominent when the knuckle joint is not flexed because when the knuckle joint is flexed. The wing area is reduced, causing much less wing area to move closer to the left-right axis. However, $C_{L_{\delta elev}}$ is increasing as the elbow is flexed, showing that the wing is capable of producing more lift when swept forward at the elbow.

4.2.2.5 Rate of Divergence

To analyze the changing stability of *Tapejara*, the largest time constant is tracked over the various configurations to give an estimate of how quickly *Tapejara* would diverge

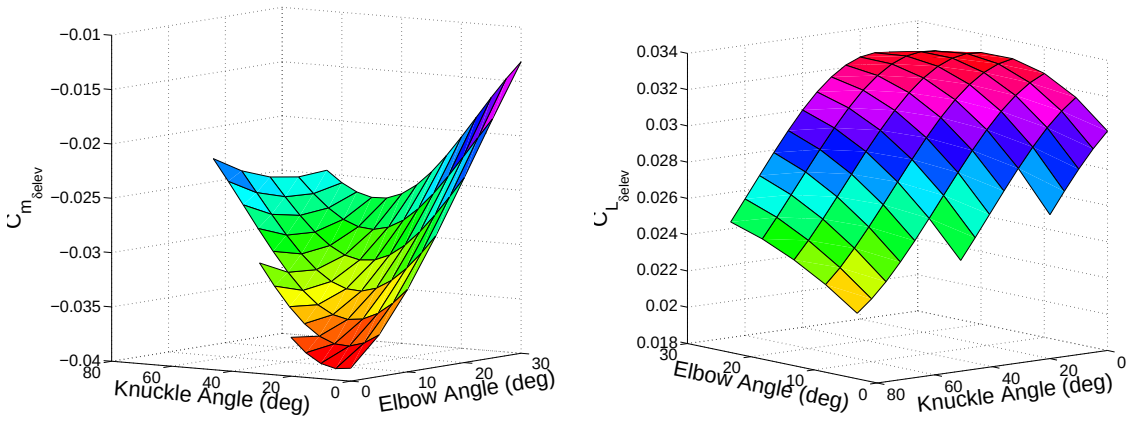

Figure 4-14. Effectiveness of Elevator in Steady Level Flight

from a steady level flight path without control actuation. As the wing is swept forward at the elbow, the largest time constant is increasing. This trend indicates that sweep forward at the elbow joint increases the rate at which *Tapejara* diverges from its trim flight condition. Increasing sweep backwards at the knuckle reduces the largest time constant, reducing the rate at which *Tapejara* diverges from its trim flight condition. Only the configurations with the knuckle flexion at its largest and elbow flexion at its smallest achieve stability.

A closer examination of the eigenvectors of the system in Table 4-3 shows that the largest time constant relates to a yaw-dominated mode. Recall that morphing at the knuckle joint greatly increases the yaw damping coefficient, C_{n_r}, as shown in Figure 5-15. So, it is not unexpected that knuckle flexion would improve *Tapejara*'s stability.

Thus, *Tapejara* could alter its stability in flight by morphing its wings, giving *Tapejara* the performance benefits that accompany instability, yet capable of soaring with less control actuation in a more stable configuration.

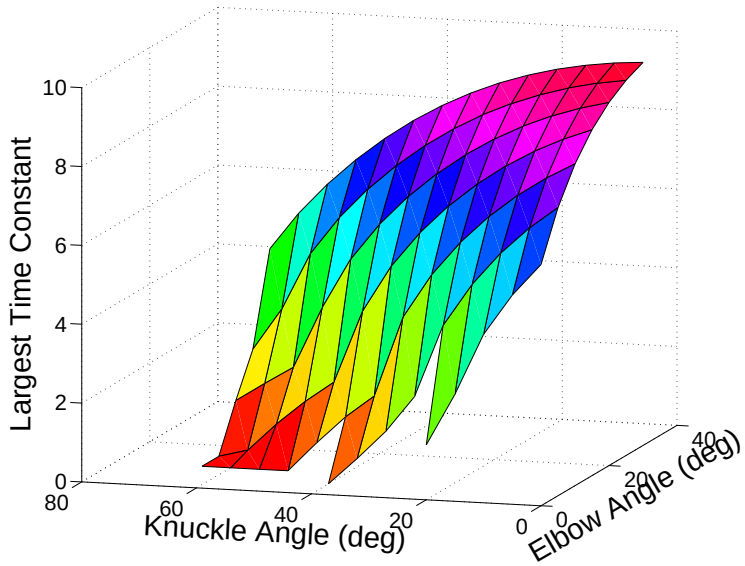

Figure 4-15. Largest Time Constant in Steady Level Flight

Time Constant	6.117
u-component	0
w-component	0
q-component	0
θ-component	0
v-component	-0.6964
p-component	-0.2189
r-component	-0.7453
ϕ-component	0.0358
x-component	0.2091e-06
y-component	0.04836
z-component	0.4510e-07
Ψ-component	0.1218

Table 4-3. Eigenvector of Nominal Configuration in Steady Level Flight

4.2.3 Head Free Asymmetric Sweep Results

The results presented in this section refer to the runs that test various asymmetric wing configurations, while allowing the head to be free to balance the yaw moments. Sideslip angle is held to zero for all cases.

4.2.3.1 Trimmed Flight Conditions

Similar to the symmetric sweeps, the amount of elevator deflection required to balance the pitching moment is decreased as the wing is swept forward. The angle of attack also decreases for the same reason as for the symmetric sweeps. The elevator deflection that is required to trim *Tapejara* follows an interesting trend as the knuckle is flexed. Elevator deflection increases as the knuckle is flexed through small angles, but the rate of change slows until it decreases as the knuckle is flexed through large angles. The trend reversal occurs because of two competing effects. As the wing area decreases due to the knuckle being flexed, a larger wing twist is required to achieve the same pitching moment. However, as the knuckle flexes, the outboard portion of the wing moves further from the center of mass along the anteroposterior axis, thus reducing the amount of force needed on the wing to counteract the pitching moment produced by the center of mass being a distance away from the center of lift. Through small angles, the loss of area on the lifting surface is the dominant factor, but eventually the change in position of the wing area causes the amount of necessary elevator deflection to drop.

Asymmetric sweep differs from symmetric sweep in that it creates yaw and roll moments, forcing rudder and aileron deflection to increase to compensate. A reduction in right wing area results in a decrease in lift on the right wing, which creates a roll moment that requires aileron deflection. The reduction in right wing area also causes the drag on the right wing to decrease; furthermore, the lift differential produces an even greater drag differential due to the induced drag effects. The large drag differential yields a yaw moment that requires a rudder deflection to compensate. Thus, the rudder and aileron follow nearly identical trends for this case.

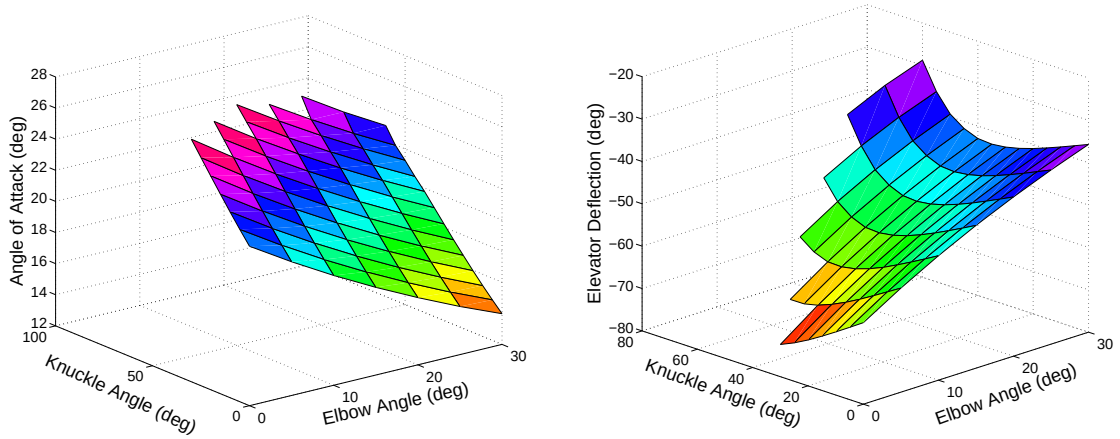

Figure 4-16. Angle of Attack and Elevator Deflection in Steady Level Flight with Head Free Asymmetric Morphing

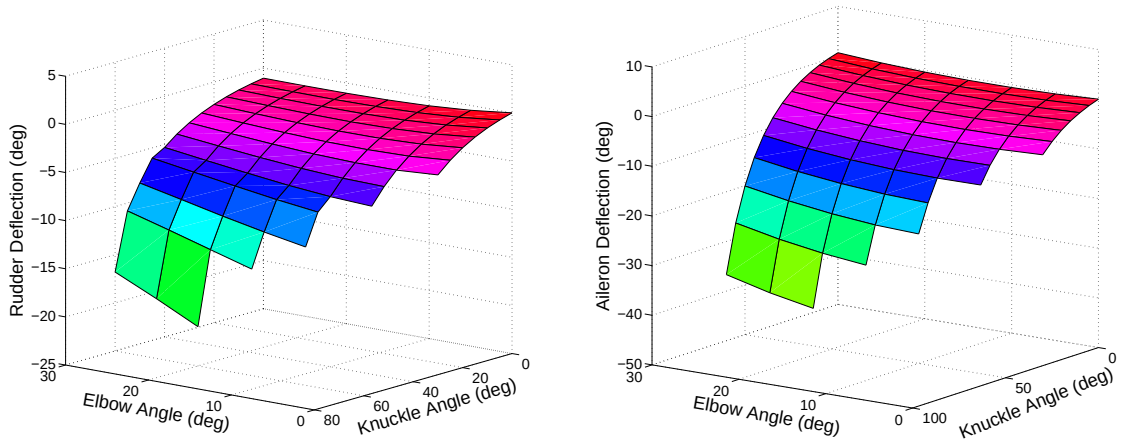

Figure 4-17. Rudder and Aileron Deflection in Steady Level Flight with Head Free Asymmetric Morphing

The control deflections of the rudder and ailerons create an even larger drag than that lost by the right wing. In fact, the rudder is by far the most dominant factor in the amount of drag created as can seen by the fact that drag increases almost exactly with increases in the magnitude of rudder deflection. Flexion at the elbow has minimal impact on the lift or drag created by the left wing; so, it has minimal impact on the head deflection, aileron deflection, or the drag created. Elbow flexion seems to reduce these trim conditions by a very small margin.

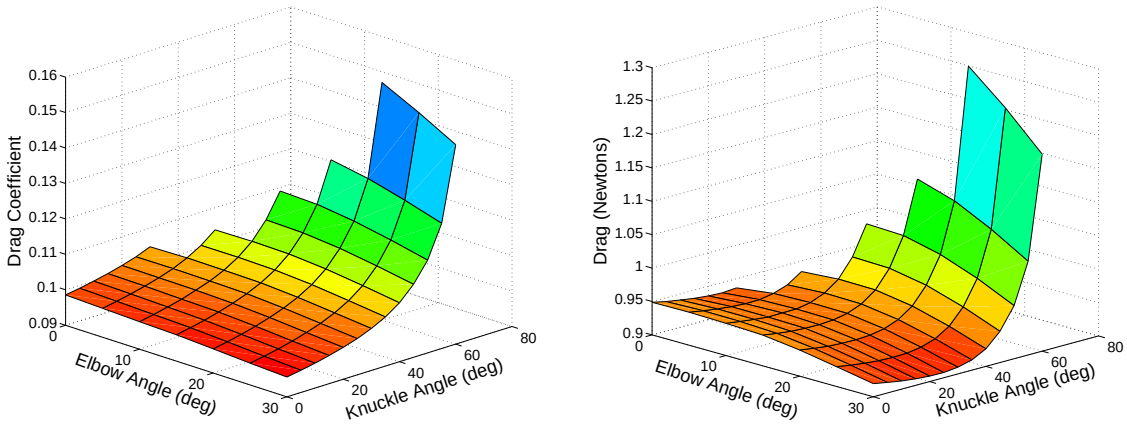

Figure 4-18. Drag and Drag Coefficient in Steady Level Flight with Head Free Asymmetric Morphing

The correlation between rudder deflection and drag shows that the aerodynamic effect of the head is extremely powerful and must be understood better to fully explain the flight phenomena of *Tapejara*. Even as the wing area of the right wing is being reduced (which typically would lead to a decrease in drag), the necessary rudder deflection for compensation is creating drag increases of 30%.

4.2.3.2 Static Stability

Static stability derivatives show similar trends with respect to asymmetric wing sweep as they did with respect to symmetric wing sweep, but on a smaller scale. For example, C_{n_β} changes from -0.1 at the nominal configuration to a minimum of -0.26 in the presence of symmetric sweep, but only reaches a minimum of -0.18 when asymmetric sweep is used. The reduction of wing area and wing moment arm that occurs when a wing sweeps backward produces the phenomena seen in both Figure 4-19 and Figure 4-9. However, in the asymmetric sweep runs only one wing sweeps backward, so the net effect is reduced.

The longitudinal dynamics behave similarly to the symmetric wing sweeps, with C_{L_α} decreasing with knuckle flexion because the wing's aspect ratio is decreasing. C_{m_α} decreases with elbow flexion because the pitching moment arm between the center of lift and the center of gravity is decreasing. The only noticeable difference is seen in the critical

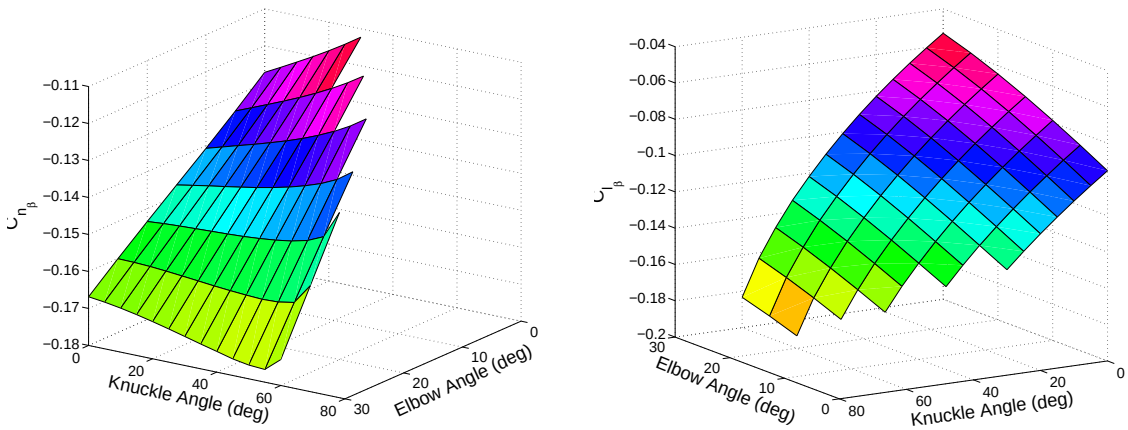

Figure 4-19. Yaw and Roll Stability in Steady Level Flight with Head Free Asymmetric Morphing

point along the curve of C_{m_α} with respect to knuckle angle. The data reaches a low point at a knuckle angle of 10° for asymmetric wing sweeps, whereas its low occurs at 50° for symmetric wing sweeps.

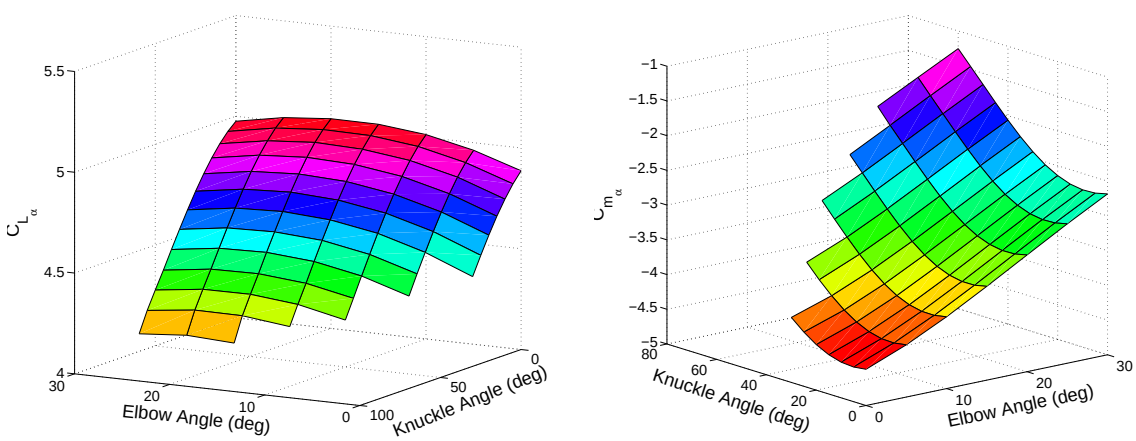

Figure 4-20. Lift Slope and Pitch Stability in Steady Level Flight with Head Free Asymmetric Morphing

4.2.3.3 Control Effectiveness

Once again, it is apparent that the effectiveness of the wing in creating roll and yaw moments and lift is reduced with increasing sweep at the knuckle joint. $C_{L_{\delta elev}}$ decreases, while $C_{L_{\delta ail}}$ increases, showing that the lift created by the right wing is reduced when the

wing twists. Meanwhile, $C_{n_{\delta rudd}}$ is becoming larger, showing that the head is becoming the more dominant factor in *Tapejara*'s dynamics. These control effectiveness metrics follow the same trends as those for symmetric wing sweeps.

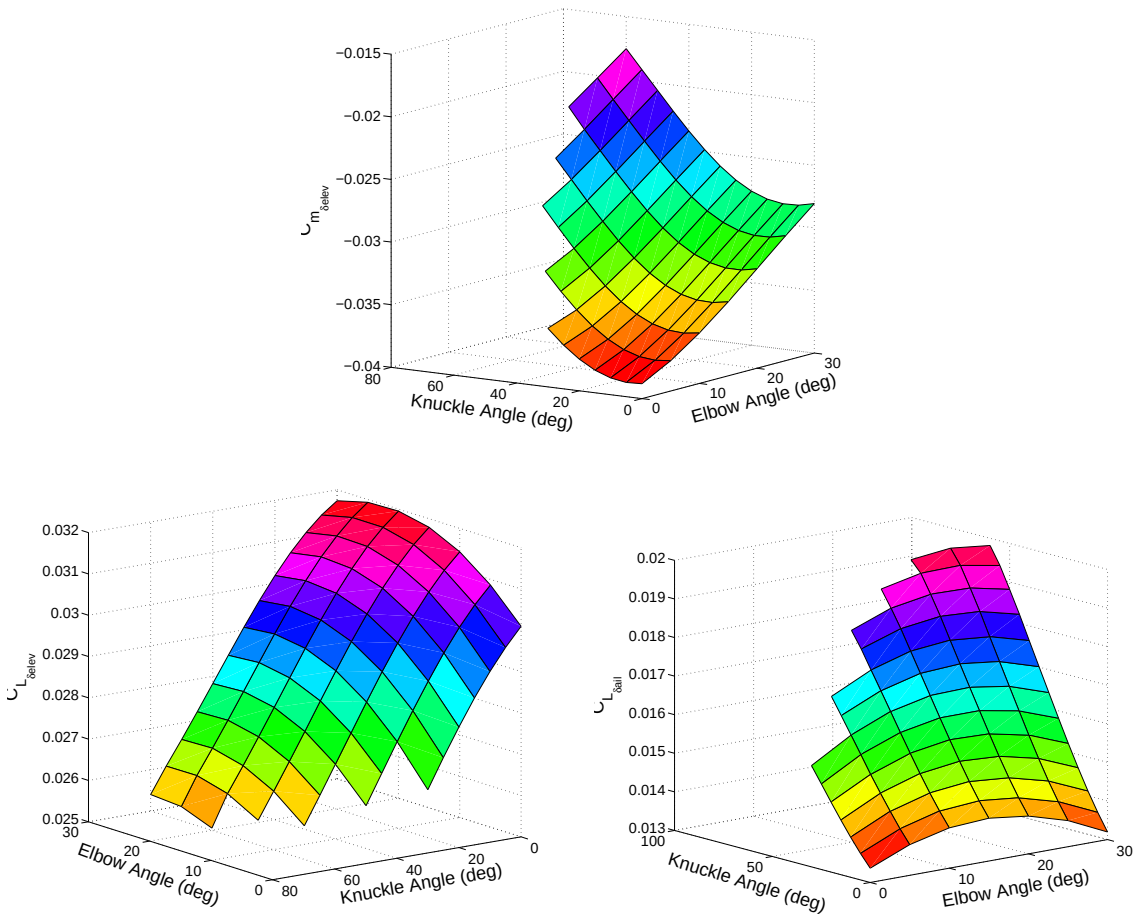

Figure 4-21. Control Effectiveness on Longitudinal States in Steady Level Flight with Head Free Asymmetric Morphing

4.2.3.4 Rate of Divergence

The same static stability and control effectiveness trends characterized asymmetric wing sweep as symmetric wing sweep, so it follows that the dynamic stability would exhibit the same trends as well.

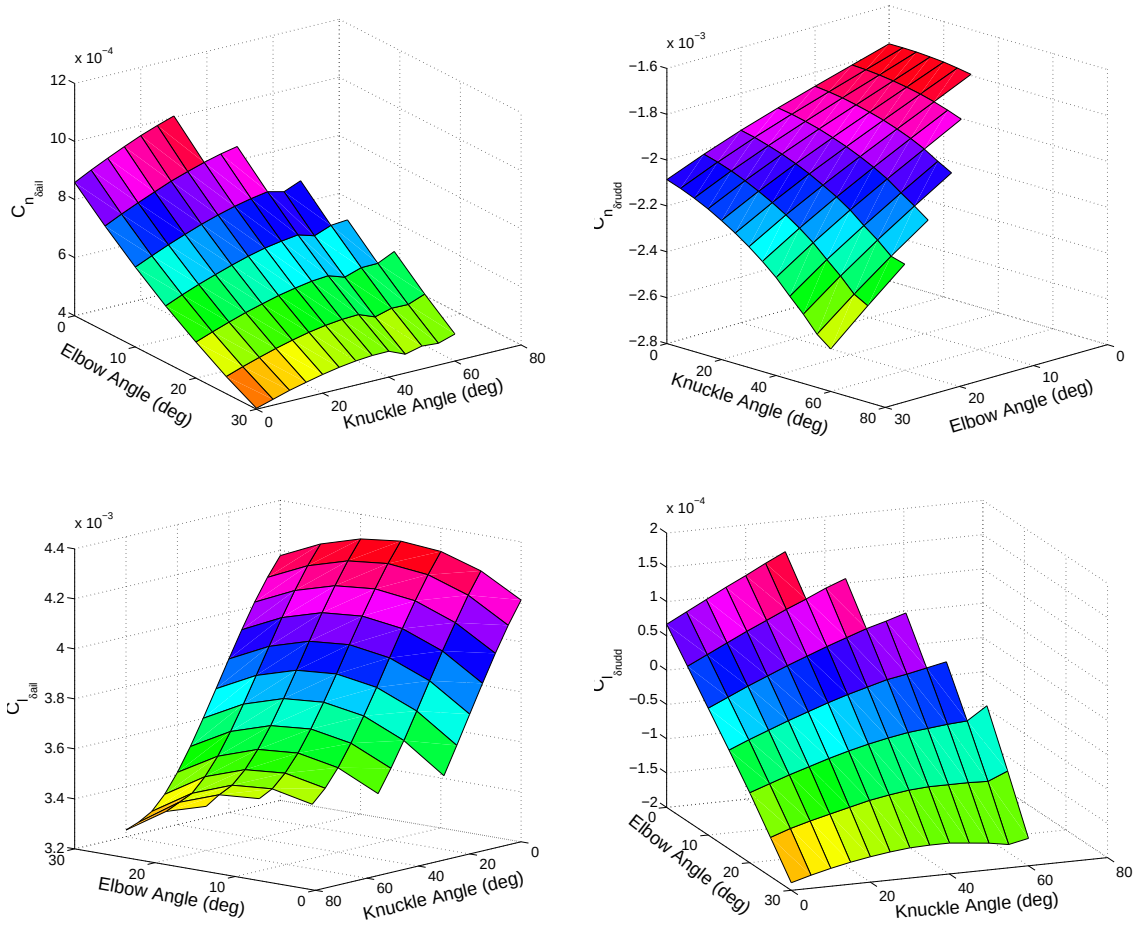

Figure 4-22. Control Effectiveness on Lateral-Directional States in Steady Level Flight with Head Free Asymmetric Morphing

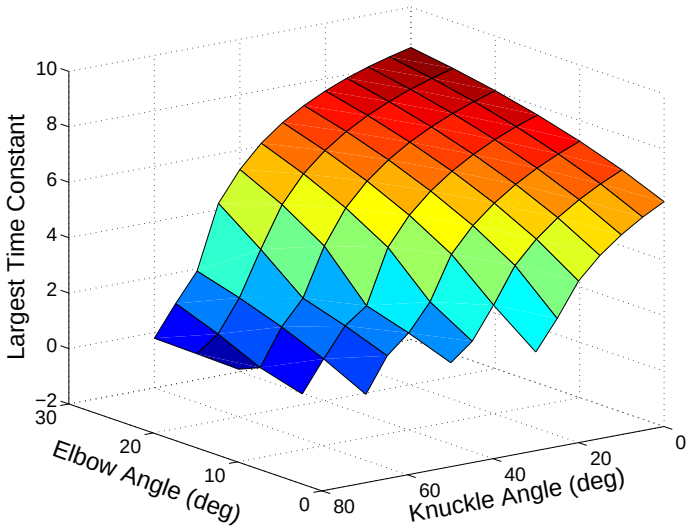

Figure 4-23. Largest Time Constant in Steady Level Flight with Head Free Asymmetric Morphing

4.2.4 Head Fixed Asymmetric Sweep Results

The results presented in this section refer to the runs that test various asymmetric wing configurations, while forcing the head to be fixed at a specified angle. Sideslip angle is allowed to vary to balance the yaw moment.

4.2.4.1 Trimmed Flight Conditions

The aileron trends seen in the asymmetric sweeps have a significant impact on the amount of sideslip needed to maintain steady, level flight when the head is held at a fixed angle. When the knuckle joint is flexed, the required aileron deflection increases to balance out the roll moment, which increases the lift on the right wing and decreases the lift on the left wing, and consequently, has the same effect on the drags of the two wings. The reduced drag differential between the two wings reduces the sideslip required to produce a yaw moment to balance out the drag differential. Elbow flexion has a minimal impact on the required sideslip, control deflections, or drag.

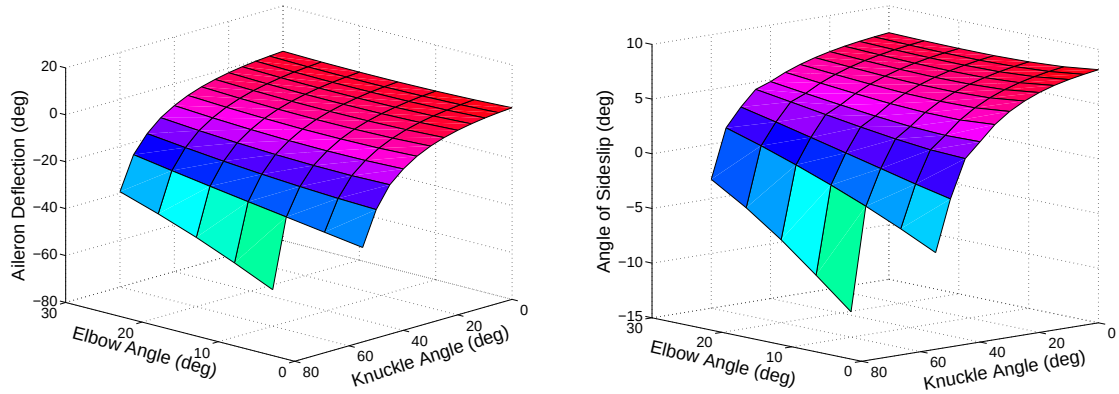

Figure 4-24. Angle of Sideslip and Aileron Deflection in Steady Level Flight with Head Fixed Asymmetric Morphing

This result demonstrates that *Tapejara* had the ability to alter its trim sideslip angle in flight by using wing morphing rather than turning its head, thus allowing its head to be free to track objects of interest.

The elevator and angle of attack plots look nearly identical to those in Figure 4-16 for the head free runs. Forcing the head into a nonzero angle, thereby producing a nonzero

sideslip angle, is a purely lateral-directional phenomenon. Thus, the forced head deflection has a negligible impact on *Tapejara*'s longitudinal flight conditions.

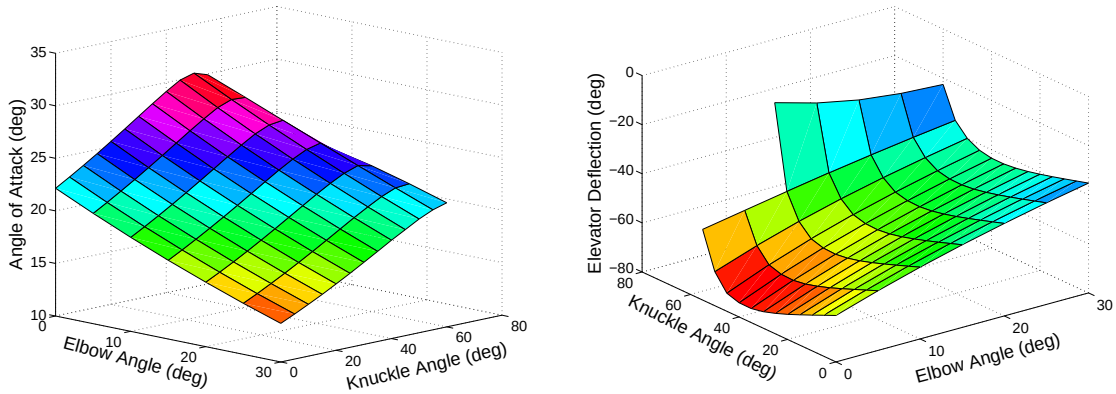

Figure 4-25. Angle of Attack and Elevator Deflection in Steady Level Flight with Head Fixed Asymmetric Morphing

Drag remains largely constant over the various asymmetric tested configurations due to competing effects between sideslip angle and angle of attack. With the head held at a fixed angle to the body, the sideslip angle determines how much that control surface is deflected into the oncoming airflow. The angle of attack dictates how much the wing surface is deflected into the airflow. Thus, these two angles are very large contributors to the drag on the vehicle. For these run cases, when angle of attack is at its lowest point, sideslip angle is at its highest value and vice-versa. This combination produces a relatively constant drag over a range of asymmetric sweep configurations.

4.2.4.2 Static Stability

Observe that sideslip angle in Figure 4-24 is nearly identical to the rudder deflection seen in Figure 4-17, except that it is offset by 10°. It is apparent that the sideslip angle is rotating *Tapejara* such that the head is at a nearly identical direction with respect to the oncoming airflow as occurs in the cases when the head is allowed to rotate freely. Thus, the only difference between the flight conditions produced by head-free and head-fixed run cases is a 10° difference between the orientation of the body and the head. A difference this small is not enough to disturb the model away from its previously held dynamics. For

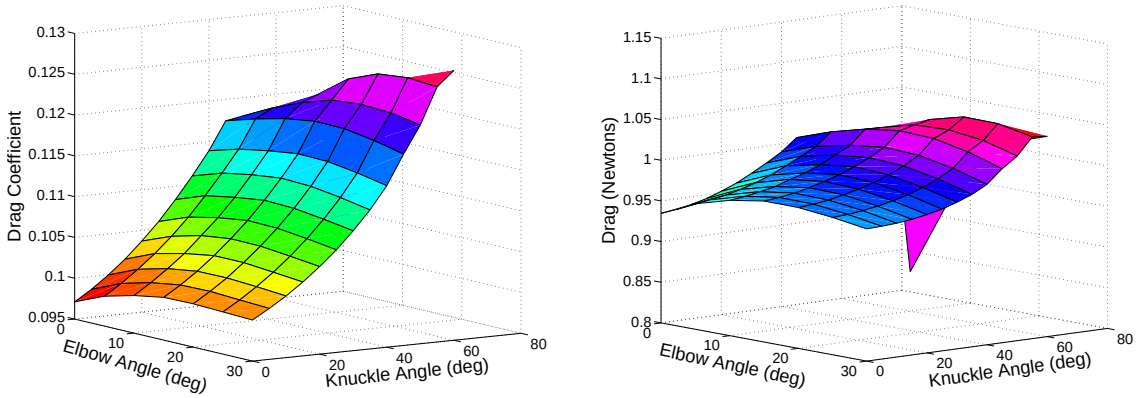

Figure 4-26. Drag Coefficient and Drag in Steady Level Flight with Head Fixed Asymmetric Morphing

this reason, the asymmetric morphing static stability derivatives are nearly identical for the head-fixed case as for the head-free.

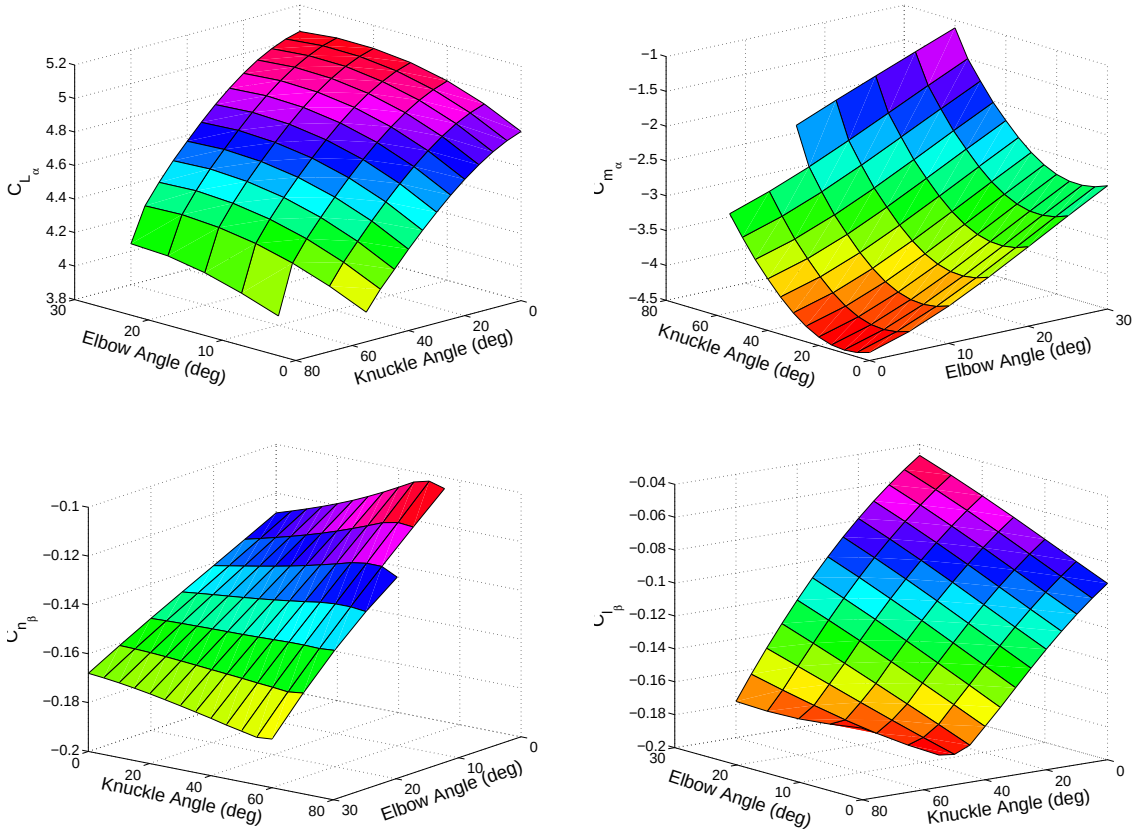

Figure 4-27. Static Stability in Steady Level Flight with Head Fixed Asymmetric Morphing

4.2.4.3 Control Effectiveness

For the same reason as described in the static stability section above, the control effectiveness trends for the head-fixed case are identical to those for the head-free case.

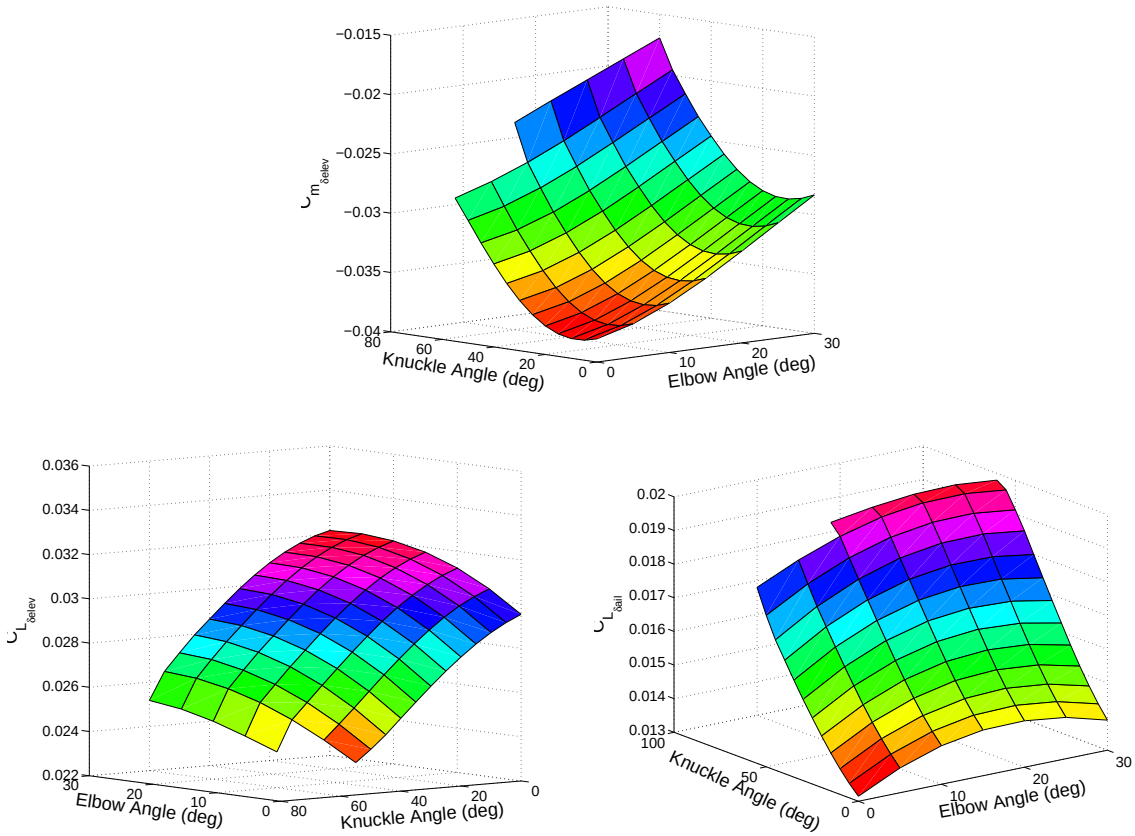

Figure 4-28. Control Effectiveness on Longitudinal States in Steady Level Flight with Head Fixed Asymmetric Morphing

4.2.4.4 Rate of Divergence

Again, the rate of divergence is seen to decrease as the wing is swept back at the knuckle and increase slightly as the elbow joint is flexed forward.

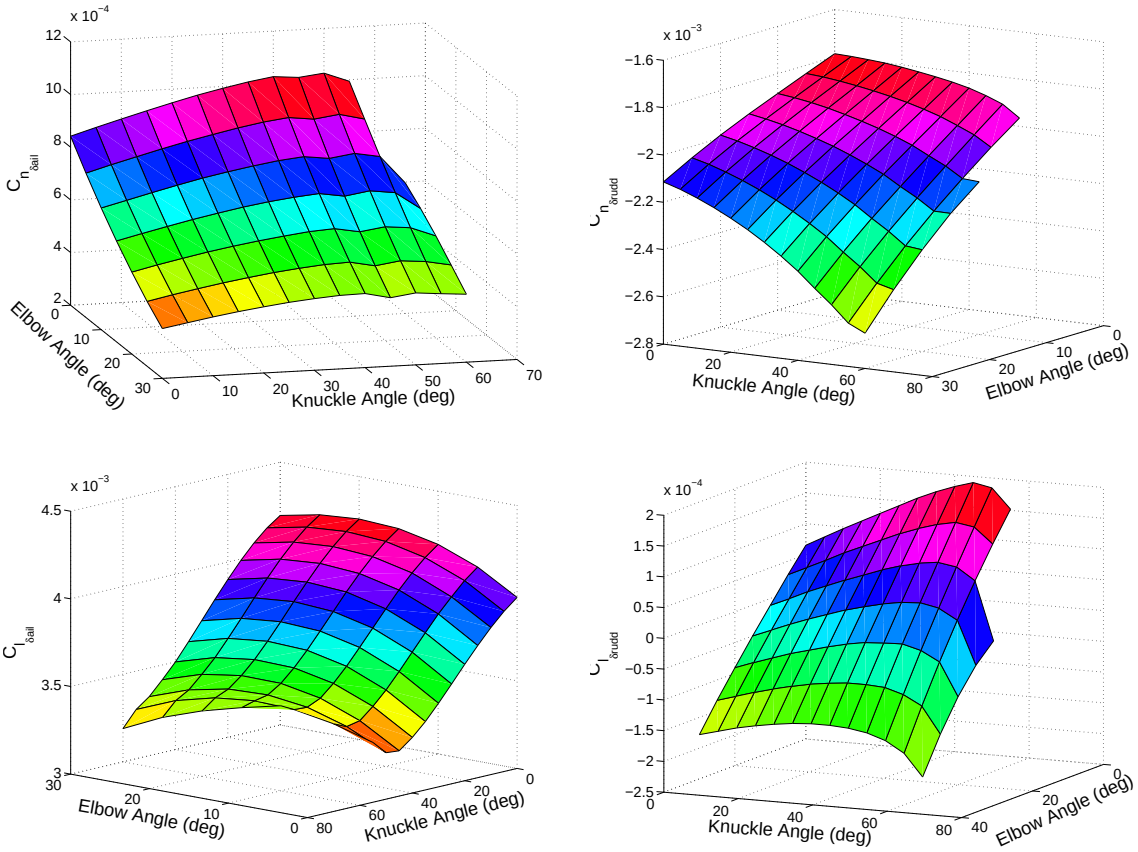

Figure 4-29. Control Effectiveness on Lateral-Directional States in Steady Level Flight with Head Fixed Asymmetric Morphing

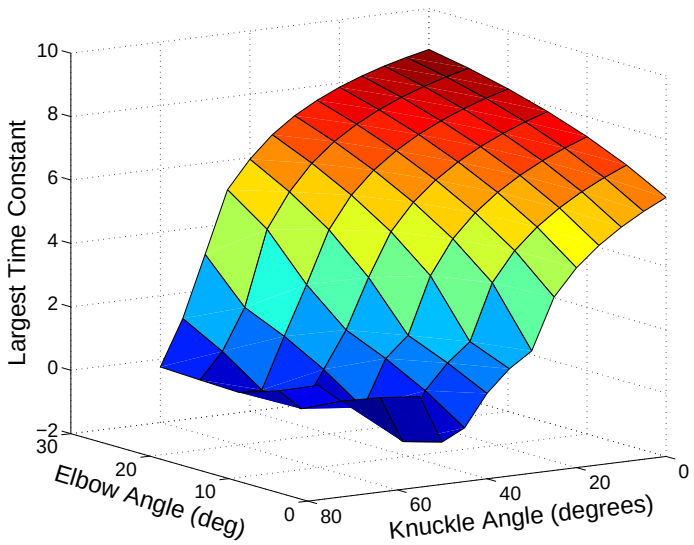

Figure 4-30. Largest Time Constant in Steady Level Flight with Head Fixed Asymmetric Morphing

4.3 Banked Turning Flight Analysis

4.3.1 Run Conditions and Analysis Methods

An analysis of turn performance is conducted to find benefits in trimmed flight performance produced by a combination of forward-placed vertical tail and wing sweep morphing. Only asymmetric wing sweep is conducted for the banked turn to find configurations that would produce the desired asymmetric yaw and roll effects that would improve turn performance. The model is analyzed at varying velocities throughout the range of asymmetric morphing configurations and with its rudder fixed at a defined angle of -10° (trailing edge left providing a yaw right moment) and bank angle set at +30° (right wing tip down creating a right turn).

Then, the output data are normalized to constant drag equal to 1 Newton. This method is justified because the research is investigating gliding flight of *Tapejara*, so the lift to drag ratio is the most important datum. If the research focused on flapping flight, then the output data would have to be normalized to *Tapejara*'s available power. Turn performance data is then derived from the velocity that produces a drag force on 1 Newton. The value of 1 Newton is chosen because it is found from test runs that the model is buffeted by a drag force of roughly 1 Newton when the velocity is 10 m/s.

4.3.2 Performance Effects

Turn radius is modestly decreased by increased elbow flexion, but has a slight tendency to increase with respect to flexion at the knuckle joint. Flexion at the elbow produces reductions of turning radius on the order of 5%. Flexion at the knuckle increases the turning radius by about 3%.

Similar trends are seen in the turn rate, with an increase in turn rate with knuckle flexion and for elbow flexion at large knuckle angle. These performance improvements are created by the decrease in velocity during the turn.

The increase in turn radius with respect to knuckle flexion makes sense, because moving the right wing area closer to the anteroposterior axis produces a roll moment that

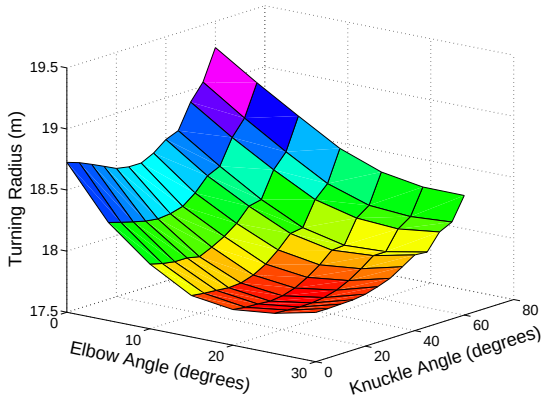

Figure 4-31. Turn Radius Improvements in Banked Flight with Asymmetric Morphing

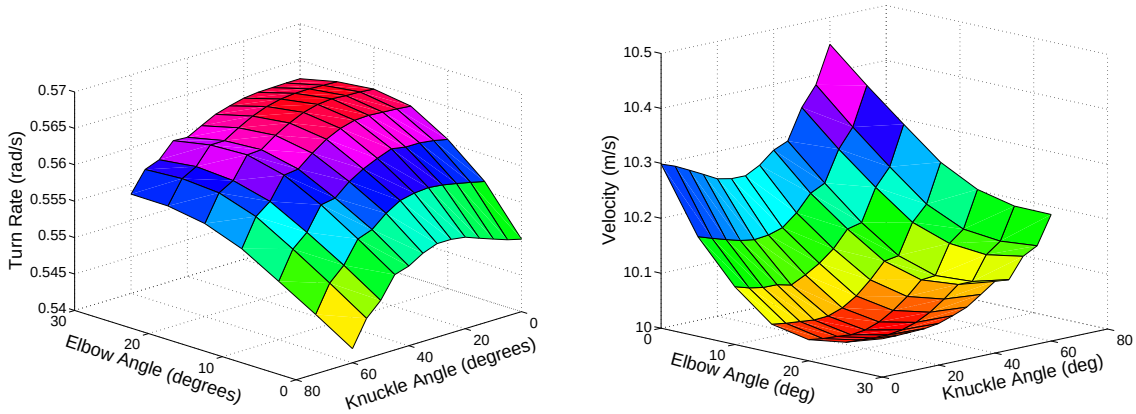

Figure 4-32. Velocity and Turn Rate in Banked Flight with Asymmetric Morphing

requires greater wing twist to hold *Tapejara*'s bank angle. The left wing is larger than the right wing, so the increased deflection produces more drag on the left wing, which yaws *Tapejara* to the left. The yaw moment combines with the roll to the right to allow *Tapejara* to make a tighter turn.

A forward sweep of the left wing would seem to benefit turn performance from the improved lift to drag seen from previous analysis. An increase in lift would roll the plane right and a decrease in drag would yaw the plane right, as well. It appears that this effect is occurring when the right knuckle angle is large, but that some other unexplained effects may be occurring when the right wing is close to its nominal position.

These results indicate that *Tapejara*'s wing morphing and forward-placed rudder affected its maneuverability and its ability to survive. A tighter turning radius would allow *Tapejara* to maneuver quicker to catch prey and avoid obstacles.

4.3.3 Trimmed Flight Conditions

The trimmed flight conditions in Figure 4-33 and Figure 4-34 support the justification for performance improvement. Sweep back at the knuckle joint of the right wing produces a lift differential that rolls *Tapejara* to the right. Negative aileron deflection counters this moment, creating more drag in the process. The lift differential between the wings is accompanied by a drag differential that creates a yaw left moment. This moment reduces the need for positive sideslip to rotate *Tapejara*'s crest out of the oncoming flow; thus, the sideslip angle decreases.

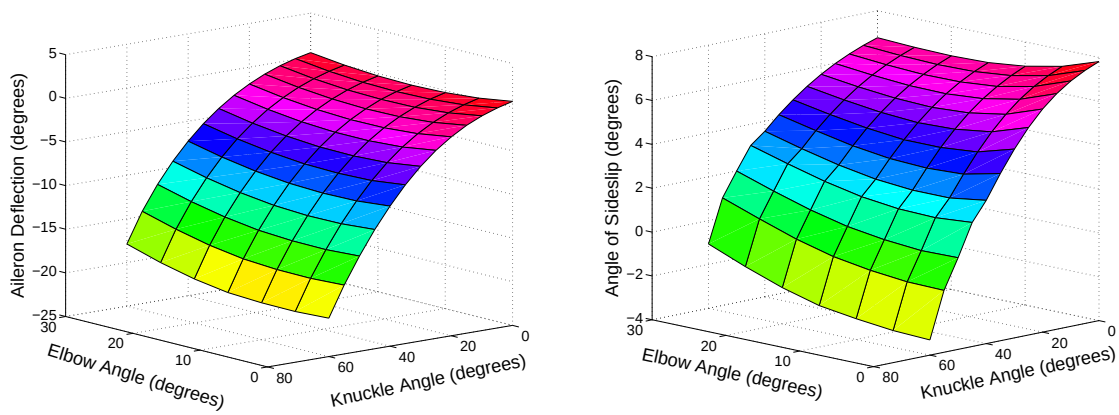

Figure 4-33. Aileron Deflection and Angle of Sideslip in Banked Flight with Asymmetric Morphing

Particularly note the increase in angle of attack and rudder deflection that occurs when the knuckle is fully flexed. The reduction in wing area created by morphing at the knuckle joint requires an increase in lift coefficient to sustain level flight. That increase in lift coefficient is accomplished by increasing the angle of attack. An increase in angle of attack creates a direct increase in drag and a pitching moment that will require more elevator deflection, creating even more drag. These escalations in drag values slow *Tapejara* down, allowing it to make quicker turns.

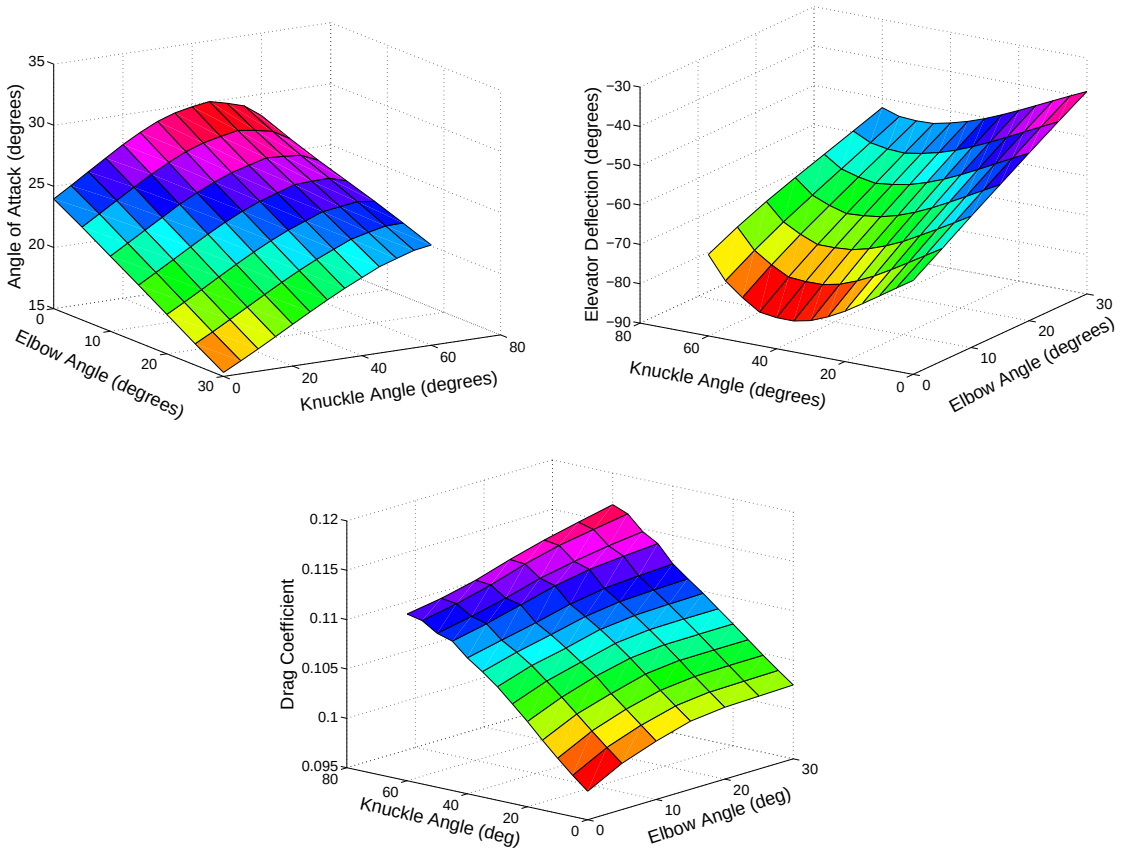

Figure 4-34. Angle of Attack, Elevator Deflection, and Drag Coefficient in Banked Flight with Asymmetric Morphing

CHAPTER 5
AICRAFT MODEL ANALYSIS

5.1 Aircraft Model

A baseline shape is determined for the vehicle. This baseline shape represents a stable vehicle that has demonstrated flight capability as a miniature air vehicle (MAV) (23). The planform and associated computational model are shown in Figure 5-1.

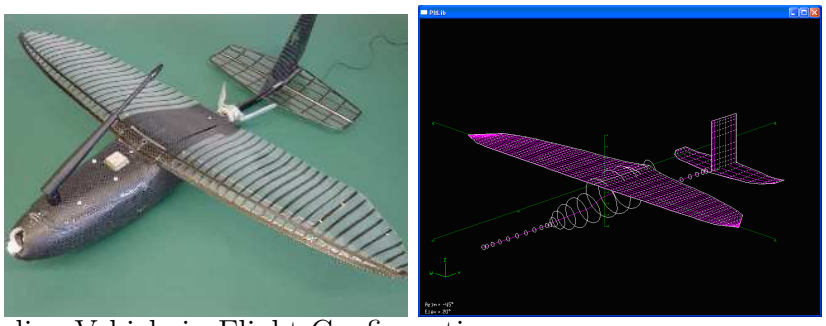

Figure 5-1. Baseline Vehicle in Flight Configuration

5.1.1 Aerodynamic Geometry

The vehicle is modeled with three lifting surfaces: wing, horizontal tail, and vertical tail. The wing and horizontal tail are left unchanged from previous analysis. The vertical tail is changed to reduce complicating factors in the analysis. Its shape is modified from having curved leading and trailing edges with spanwise chord variations to a simple rectangle of the same surface area and span, thereby making the chord constant and equal to the mean chord of the original vertical tail. The airfoils used on each surface are left unchanged from the original design. As mentioned before, AVL does not take airfoil thickness into account, so all that matters is the camber line. The wing has a maximum of 8% camber located at 30% along the chord. The two tails have symmetric airfoils.

The vehicle has three distinct bodies: fuselage, aft tail boom, and fore tail boom. The original design does not have a tail boom in front of the fuselage, but it is necessary to add this to the design to allow vertical tail placement in front of the fuselage

The specific parameters of the vehicle are given in Table 5-1.

Parameter	Value
Wingspan:	31.6 in
Wing Area:	146.5 in^2
Reference Chord:	4.7 in
Center of Gravity	[-0.5, 0.0, -1.25] in
Vertical Tail Area:	13.0 in^2
Vertical Tail Chord Length:	2.9 in
Vertical Tail Span:	4.5 in
Horizontal Tail Area:	29.4 in2
Horizontal Tail Chord Length:	3.3 in
Horizontal Tail Span:	11.5 in
Fuselage Length:	11.6 in
Fuselage Width:	3.8 in

Table 5-1. Characteristics of the Baseline Vehicle

5.1.2 Masses and Inertias

The weights and inertias are measured or estimated from the actual components that are installed on the baseline aircraft, and have not been altered for the new design. The fore tail boom is the only part added to the design, so it is estimated to have the exact same mass and inertia properties as the aft tail boom. The vertical tail's inertial properties are changed to reflect its current rectangular shape. As the vertical tail is deflected and moved, its center of mass is moved in the program.

Body Part	Mass (g)	I_{xx} (gcm^2)	I_{yy} (gcm^2)	I_{zz} (gcm^2)	I_{xy} (gcm^2)	I_{xz} (gcm^2)	I_{yz} (gcm^2)
Fuselage	295	903	903	0	0	0	0
Battery	130	398	249	813	0	-569	0
Motor	50	113	1125	1013	0	-338	0
Left Wing	45	2833	64	2897	427	0	0
Right Wing	45	2833	64	2897	-427	0	0
Vertical Tail	8	0	1458	1458	0	0	0
Horizontal Tail	8	72	1530	1458	0	324	0
Aft Tail Boom	15.0	135	1219	1084	0	383	0
Fore Tail Boom	15.0	135	1219	1084	0	383	0

Table 5-2. Masses and Inertias of Modeled Aircraft Parts

5.1.3 Control Effectors

The control surfaces consist of a standard elevator, pair of ailerons, and a rudder. The elevator and aileron control surfaces are kept the same as they were for the original aircraft model. The elevator is defined, chordwise, as the aft 57% of the horizontal tail, along its entire span. The ailerons are defined, chordwise, as the aft 50% of the wing, along the outermost 40% of the wingspan. The rudder is defined as the entire vertical tail surface, rotated about its leading edge axis, so that rudder deflections match the effect of vertical tail rotations that the program executes when changing the tail's incidence angle. The model is shown below with the camber lines for the surface and the camber lines of the control surfaces.

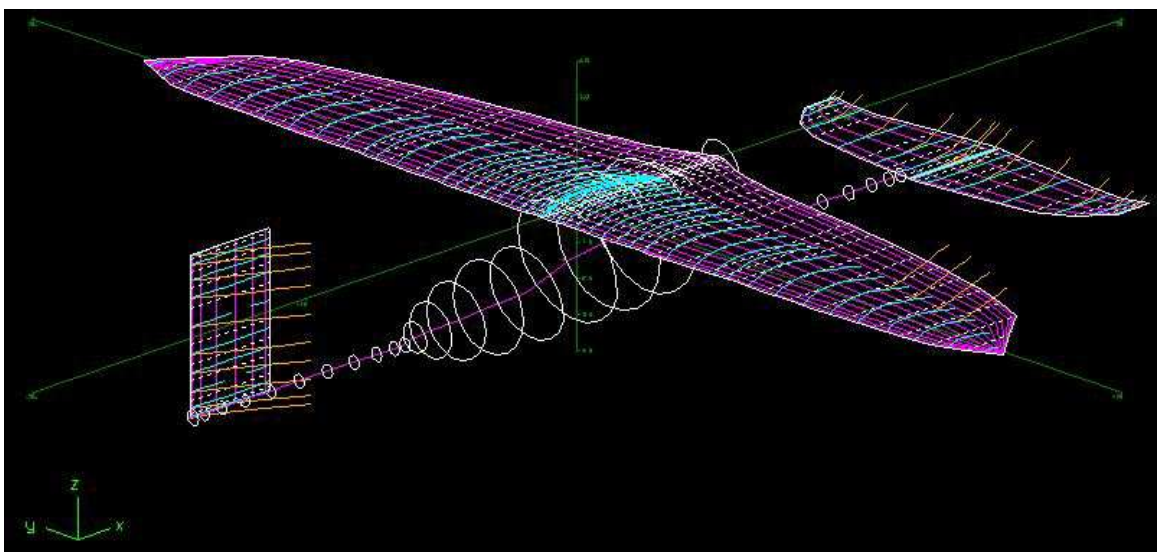

Figure 5-2. Aerodynamic Model

5.1.4 Adaptive-Configuring Vertical Tail

This project presents a revolutionary change in vehicle design by demonstrating configurations that have never been flown. Specifically, the location of the vertical tail will range far beyond the standard placements. Consider that the vast majority of aircraft either have the vertical tail pointing out the top of the rear fuselage or else have no tail whatsoever; conversely, this vehicle will include a vertical tail that can slide forward/back along the fuselage and up/down through the nose as shown in Figure 5-3.

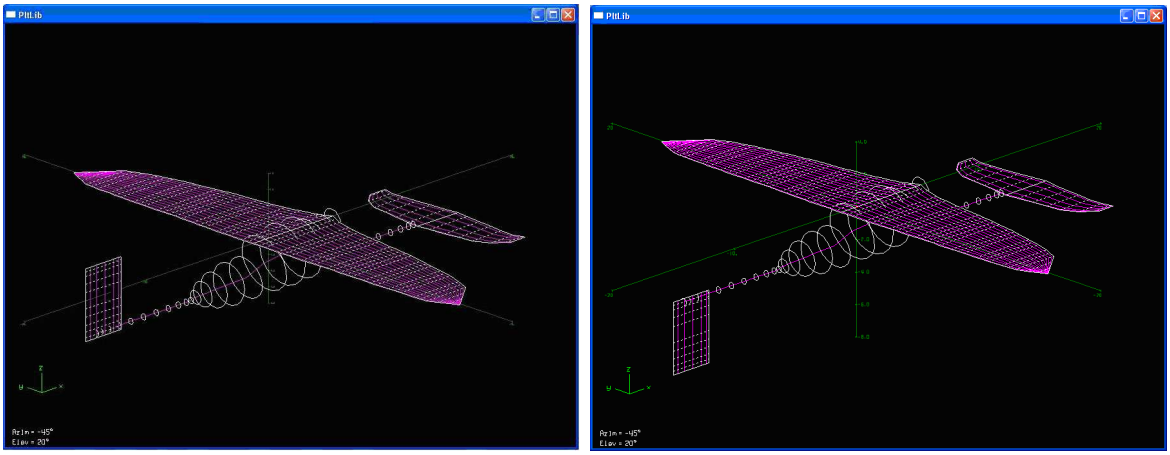

Figure 5-3. Configurations with Vertical Tail at the Nose

The purpose of a vertical tail is a critical element of any aircraft design. The traditional placement of a vertical tail that points up is chosen to provide static stability in both roll and yaw axes. A tailless vehicle lacks that stabilizing contribution so the wing sweep is increased to provide a stabilizing influence in roll and yaw. In each case, the design is focused on stability.

This novel vehicle will actually focus on agility as its metric for design. As such, the vertical tail will be placed to enhance mission performance rather than static stability. This tradeoff between performance and stability is certainly well known in the design community so morphing provides an ability to alter that tradeoff during flight.

5.2 Steady Level Flight Analysis

5.2.1 Run Conditions

The aircraft model is tested for varying vertical tail positions at a constant velocity of 24 m/s. The vertical tail is placed through a range of positions along both the vertical and longitudinal axes. The vertical tail varies in longitudinal position from 14 inches forward to 14 inches aft of the center of mass of the aircraft. The tail varies in vertical position from 5 inches above to 5 inches below the center of mass. The locations specified in the resulting plots locate the center of the rectangular vertical tail.

The elevator deflection is constrained to balance the pitch moment, the ailerons are deflected to balance the roll moment, and the rudder is used to hold the yaw moment to zero. The angle of attack is constrained to provide the necessary lift coefficient for steady level flight and the angle of sideslip is held to zero.

5.2.2 Trimmed Flight Conditions

In steady level flight the model's trimmed flight conditions show no change with respect to the vertical position of the vertical tail and little change with respect to the longitudinal position of the vertical tail. When it is moved forward, the angle of attack increases, the elevator deflection decreases, and drag increases. However, all of these changes are minimal and, due to their linear nature, are likely the result of the movement of the model's center of mass as the vertical tail moves. As the center of mass moves forward, the required elevator deflection to balance the pitch moment decreases, also decreasing the lift produced by the elevator. This effect increases the angle of attack necessary to create sufficient lift to hold the plane level, thus increasing the drag on the model.

5.2.3 Static Stability

The static stability derivatives show more significant changes. C_{m_α} becomes slightly more stable as the vertical tail moves forward and no change as the tail moves vertically. The changes in pitch stability are due to the inertial effects of moving the

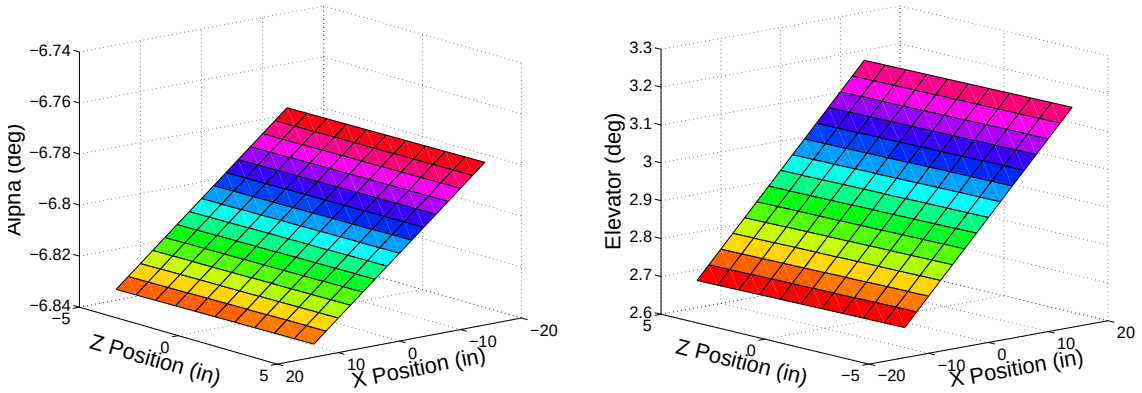

Figure 5-4. Steady Level Angle of Attack and Elevator Deflection

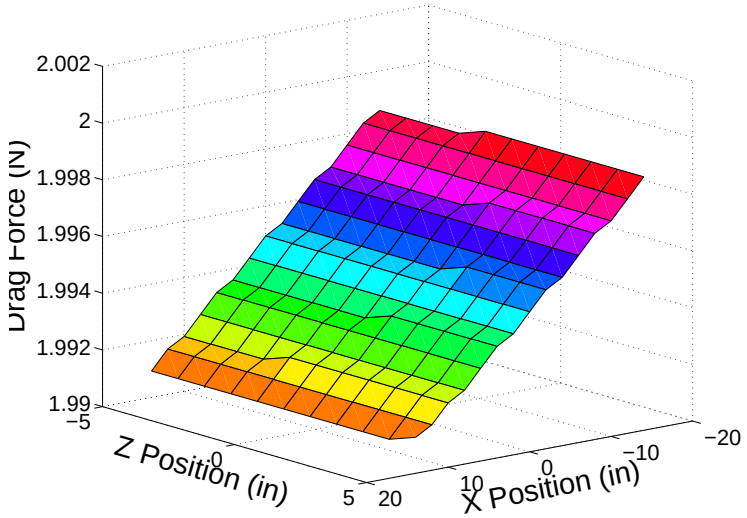

Figure 5-5. Steady Level Drag

mass longitudinally. It makes sense that the position of the vertical tail, a predominantly lateral-directional flight control surface, would have little impact on longitudinal stability; thus, the aircraft remains pitch-stable for all tested vertical tail positions in both the longitudinal and vertical directions.

The coefficient of roll moment with respect to sideslip as shown in Figure 5-7 shows a more dominant relation with respect to vertical position of the vertical tail, increasing as the tail moves down, and a slight trend towards increasing as the tail moves forward.

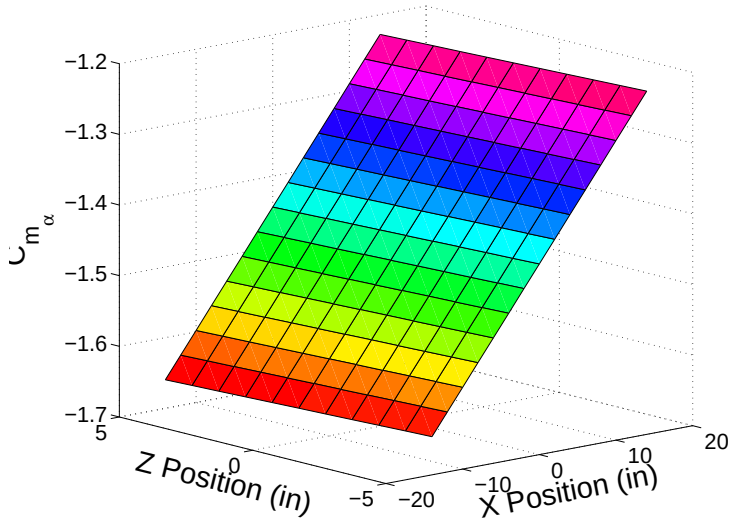

Figure 5-6. Steady Level Pitch Stability

However C_{l_β} also shows some peculiar nonlinearities in the region near the origin, indicating that some coupling or interference effects occur when the vertical tail is near the fuselage. Away from the origin, C_{l_β} becomes increasingly stable as the vertical tail moves up, and to a lesser extent, as the vertical tail moves forward. The trend with respect to the vertical position of the vertical tail follows intuitively from the recognition that the vertical tail's effect on roll moment comes from the size of the vertical tail and its rolling moment arm length, essentially the distance from the aerodynamic center of the vertical tail to the aircraft's center of mass along its vertical axis. However, the slight correlation with respect to longitudinal position does not seem to have a direct relation and could be created from some aerodynamic body/surface interactions. The end result is that the aircraft is only roll stable when the vertical tail is placed far above and behind the aircraft's center of mass and is increasingly unstable when moved down and forward.

The coefficient of yawing moment with respect to sideslip angle as shown in Figure 5-8 is nearly constant as the vertical tail is moved up and down. However, it increases linearly as the vertical tail position is moved further aft along the longitudinal axis. It is easy to understand that as the vertical tail moves vertically, the yawing moment

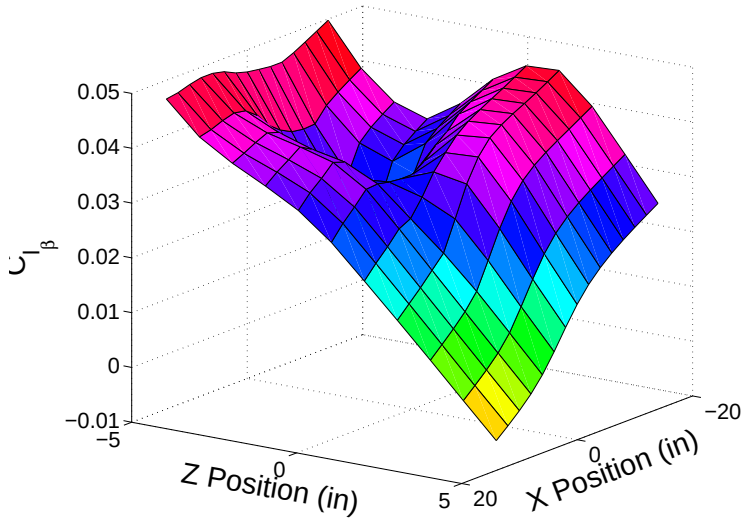

Figure 5-7. Steady Level Roll Stability

will not be impacted, because the primary factors affecting the yawing moment created by the vertical tail are the tail's size, ie. the force induced at the vertical tail by a sideslip, and the vertical tail's yawing moment arm, which is essentially the distance from the aerodynamic center of the vertical tail to the aircraft's center of mass along the longitudinal axis; hence, the strong correlation between longitudinal position and C_{n_β}. The aircraft is yaw-stable for vertical tail positions sufficiently behind the aircraft's center of mass and increasingly unstable as the vertical tail moves farther forward.

5.2.4 Rotation Damping

Roll damping coefficient exhibits very little change with respect to the position of the vertical tail. Its effectiveness increases slightly as the tail moves up and backward. On the other hand, yaw damping coefficient changes substantially with longitudinal position of the vertical tail and is nearly symmetric about the origin. The effectiveness of the vertical tail in slowing a yaw spin depends on the vertical tail's size and distance from the vertical axis through the model's center of mass. If the vertical tail is located near the center of mass, then it experiences little crosswind as the aircraft rotates, providing little moment opposing the rotation. On the other hand, if the vertical tail is located either far forward

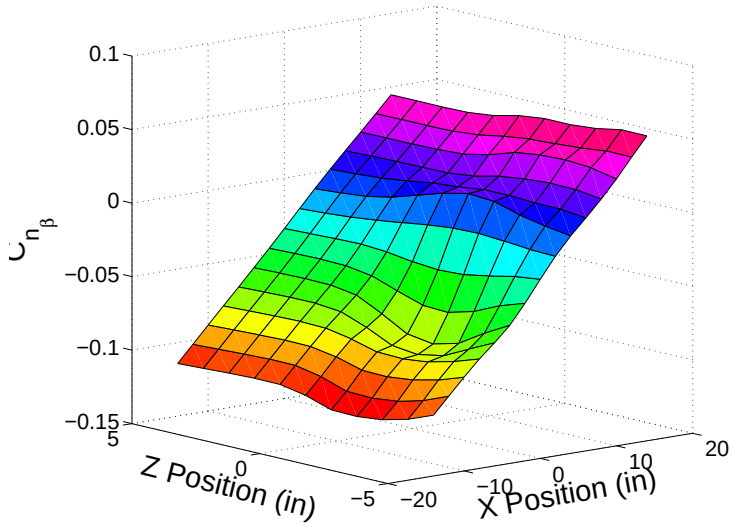

Figure 5-8. Steady Level Yaw Stability

or far aft of the center of mass, then it experiences much greater crosswind, and thus provides a much larger restoring moment.

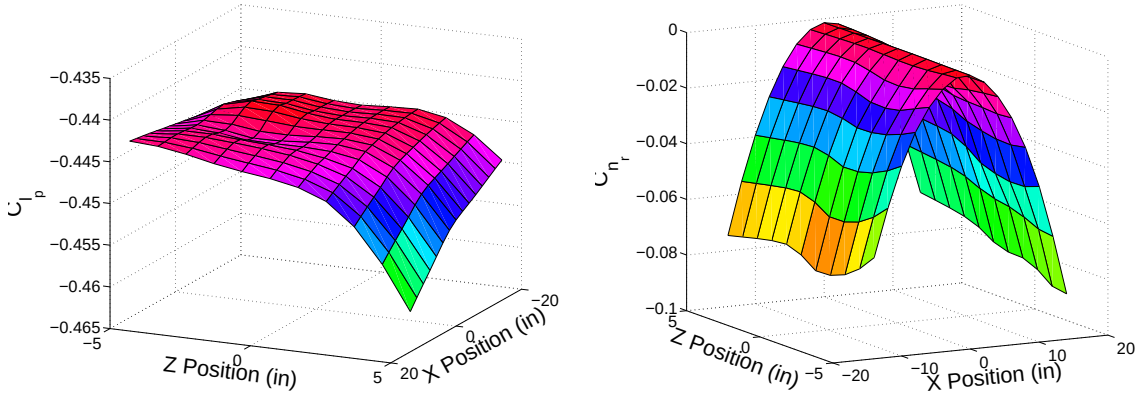

Figure 5-9. Steady Level Roll and Yaw Damping

5.2.5 Control Effectiveness

The model's pitching moment coefficient with respect to elevator deflection increases very slightly in effectiveness as the vertical tail moves forward. This trend is due to the decrease in elevator deflection seen in Figure 5-4. As any control surface deflection decreases, it effectiveness increases.

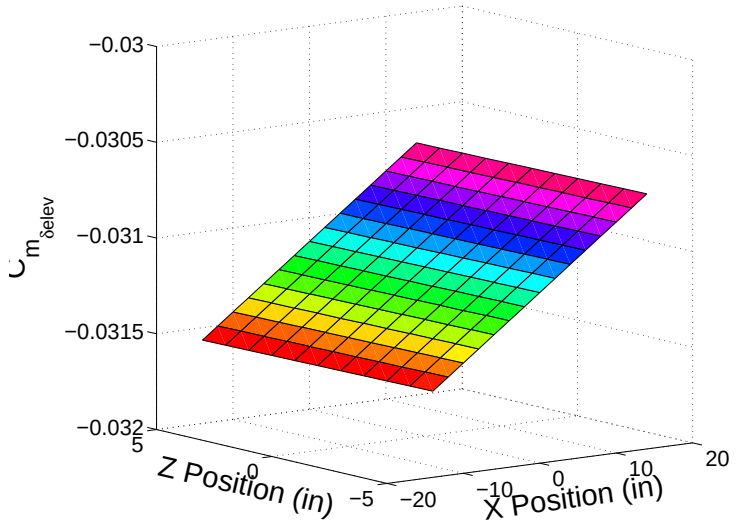

Figure 5-10. Elevator Pitch Moment Effectiveness

The effectiveness of ailerons to affect the roll moment of the aircraft barely changes in a nonlinear fashion as the vertical tail moves. The ailerons are the most effective when the vertical tail is farthest forward, and least effective when the tail is farthest aft and highest. The rudder also produces a roll moment, but can produce roll moments of opposite direction, depending on whether the vertical tail is placed above or below the center of mass. The trend is slightly nonlinear, but the vertical placement of the tail is the dominant factor.

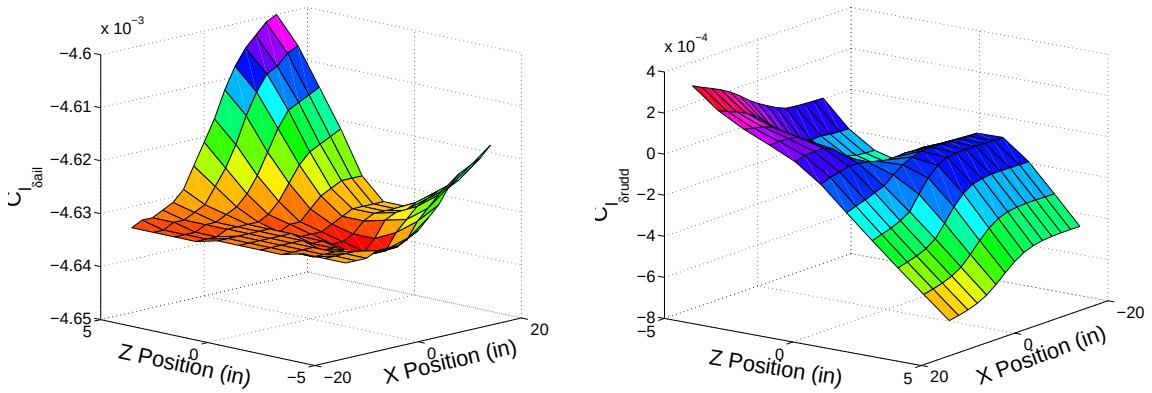

Figure 5-11. Control Surface Roll Moment Effectiveness

Aileron effectiveness on yaw moment exhibits an unusual relationship with vertical tail placment. Its effectiveness is unaffected by any placement changes when the tail is forward of the center of mass, but increases as the vertical tail moves down when the tail is aft of the center of mass. However, its effect on yaw moment is still an order of magnitude smaller than that of the rudder, which can produce yaw moments in opposing directions, depending on whether the vertical tail is located forward or aft of the center of mass. The rudder's effectiveness with respect to yaw moment is not affected by its vertical placement.

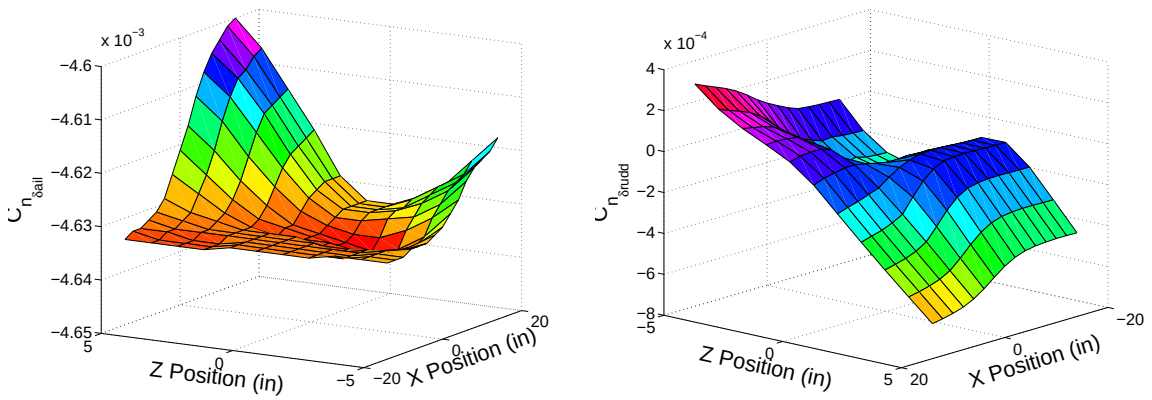

Figure 5-12. Control Surface Roll Moment Effectiveness

5.3 Banked Turning Flight

5.3.1 Run Conditions

The vertical tail is placed through the same range of positions along both the vertical and longitudinal axes for the turning flight analysis as the steady level flight analysis. The vertical tail varies in longitudinal position from 14 inches forward to 14 inches aft of the center of mass of the aircraft. The tail varies in vertical position from 5 inches above to 5 inches below the center of mass. The locations specified in the resulting plots locate the center of the rectangular vertical tail.

The elevator deflection is constrained to balance the pitch moment and the ailerons are deflected to balance the roll moment. However, in turning flight, the model is also analyzed at varying vertical tail incidence angles. These variations are used to find performance effects from rudder deflections. Consequently, the angle of sideslip is constrained to balance the yaw moment, resulting in non-zero sideslip angles. The angle of attack is still constrained to provide the necessary lift coefficient to maintain altitude.

Care is taken to change the vertical tail incidence angle rather than the rudder deflection to ensure that the correct dynamics are captured. If instead, a rudder angle is specified, then even though the aircraft configuration may be identical, the program will treat it as a control input rather than a geometric change; so, AVL's output dynamics would be identical to those of an undeflected vertical tail.

5.3.2 Performance Improvements

To analyze turning performance, the model is tested at a range of longitudinal and vertical placements of the vertical tail, a range of vertical tail incidence angles, and a range of velocities. The model's thrust production capabilities are assumed to be a constant of 2 Newtons. So, to normalize the performance metrics against each other, the velocity is found for each configuration that produces a drag force of 2 Newtons.

Turning radius is constant with respect to vertical and longitudinal placement of the vertical tail at a constant incidence angle.

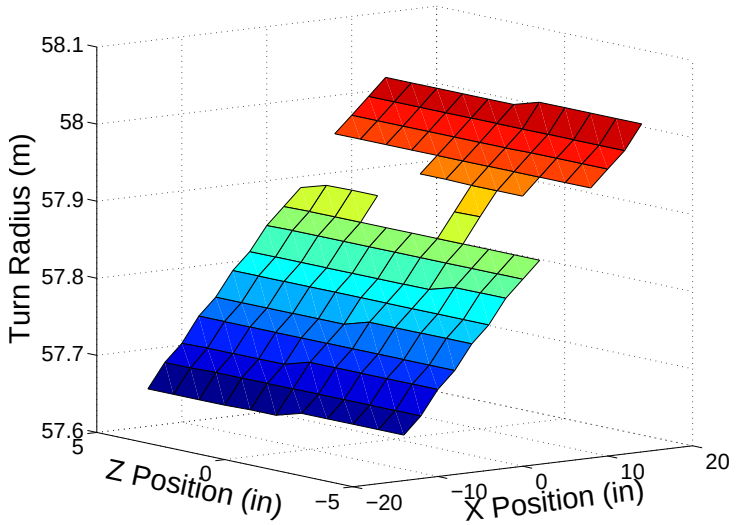

Figure 5-13. Turning Radius Changes with respect to Vertical Tail Longitudinal and Vertical Placement

When turn radius is examined with respect to the deflection and vertical placement of the vertical tail at a constant longitudinal position, a distinct trend is discernible with respect to the deflection of the vertical tail, but none is seen with respect to the vertical position.

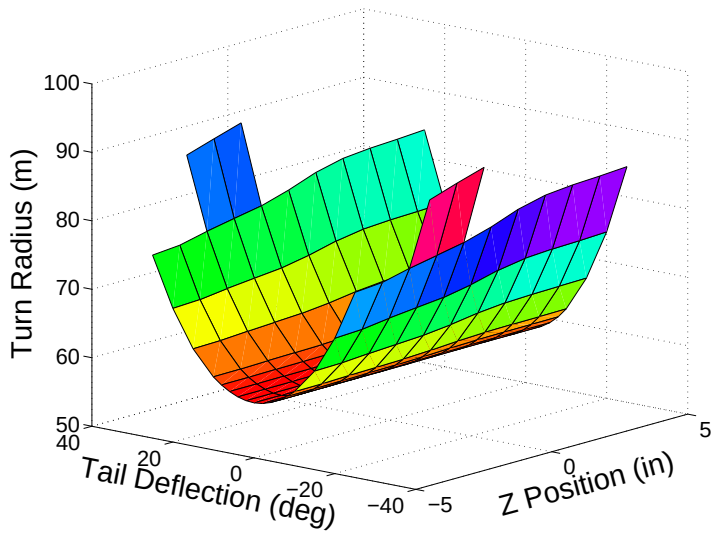

Figure 5-14. Turning Radius Changes with respect to Vertical Tail Deflection and Vertical Placement

It has been shown that turn performance is not affected by the vertical placement of the vertical tail, so this independent variable is ignored for the rest of the analysis. The true potential for turn performance improvement is finally seen when turn radius is examined with respect to longitudinal position and deflection of the vertical tail at a constant vertical location. This combination of variables shows a reduction in turn radius when the vertical tail is deflected at a forward location, but an increase in turn radius when deflected at an aft location.

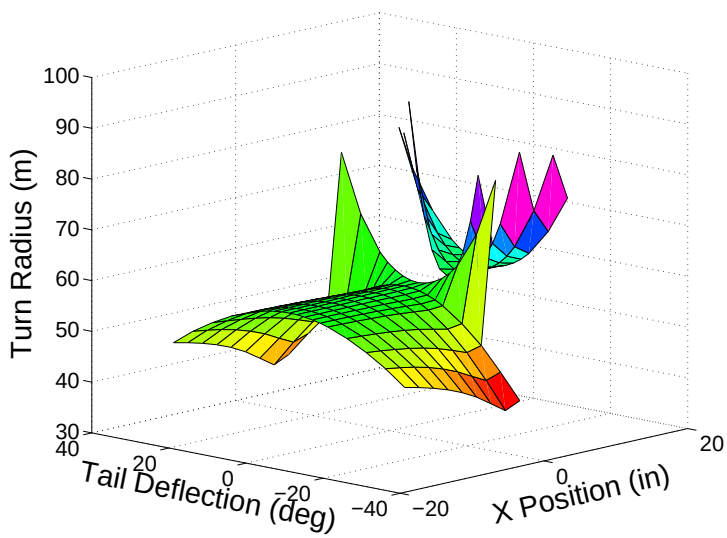

Figure 5-15. Turning Radius Changes with respect to Vertical Tail Deflection and Longitudinal Placement

The values of turn radius are extracted from Figure 5-15 at configurations with the largest values of position and angle for the vertical tail. These values, as given in Table 5-3, clearly demonstrate that placing the vertical tail over the nose has a lower radius and thus greater agility as compared to placing the vertical tail in the traditional location over the rear. Note again that the coordinate system uses a positive value towards the rear and a negative value towards the nose.

The reduction in turn radius is caused by a decrease in the velocity that creates 2 Newtons of drag. This decrease in velocity also produces an increase in turn rate.

	Angle of -25°	Angle of 0°	Angle of +25°
Rear Placement (x=+14 in)	84.43 m	58.02 m	84.05 m
Forward Placement (x=-14 in)	50.40 m	57.65 m	50.31 m

Table 5-3. Turn Radius in m at Extremal Values of Position and Angle for the Vertical Tail

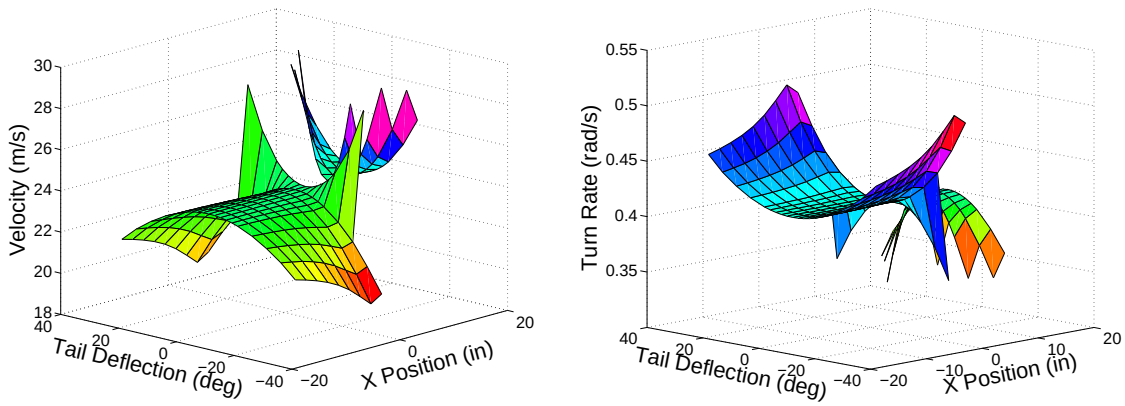

Figure 5-16. Velocity and Turn Rate in a 45° Banked Turn

These performance improvements could be expected for jet powered aircraft and for gliding flight. However, much of the current MAV fleet use propellers and electric motors for propulsion. To address this issue, the data analysis is repeated while normalizing the required power to maintain level flight. Figure 5-17 shows that similar improvements occur when the data is normalized for constant available power.

5.3.3 Trimmed Flight Conditions

In banked turning flight, the vertical tail incidence angle is fixed, so the sideslip angle changes to balance the yaw moments. Flight conditions are examined with respect to longitudinal position and angle of deflection of the vertical tail. It was observed previously that the vertical position of the vertical tail had little to no impact on turning performance metrics, but that both the longitudinal placement and deflection of the vertical tail did, so the trim conditions are found at a variety of longitudinal positions and deflection angles. Just as in the performance metric analysis, all flight conditions are found at a speed that produces 2 Newtons of drag.

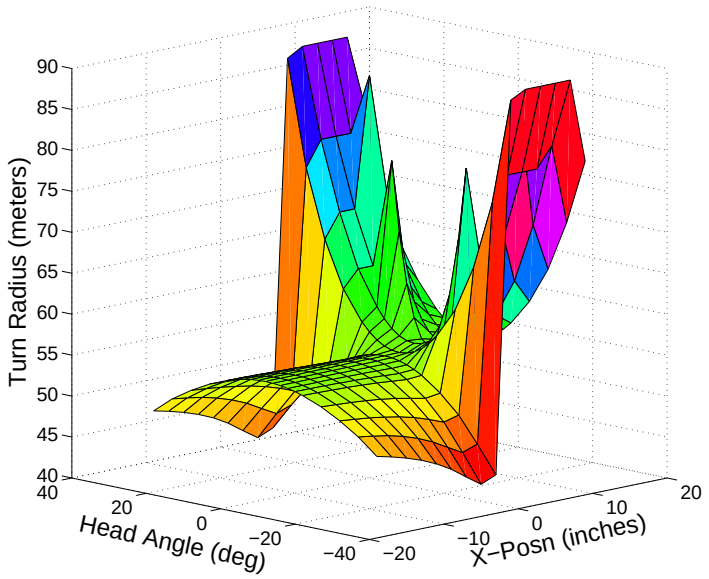

Figure 5-17. Power Normalized Turning Radius Improvements

The dominant trend seen in angle of attack is to increase as the vertical tail deflection increases. This increase in angle of attack produces a decrease in the required elevator deflection to balance the pitching moment.

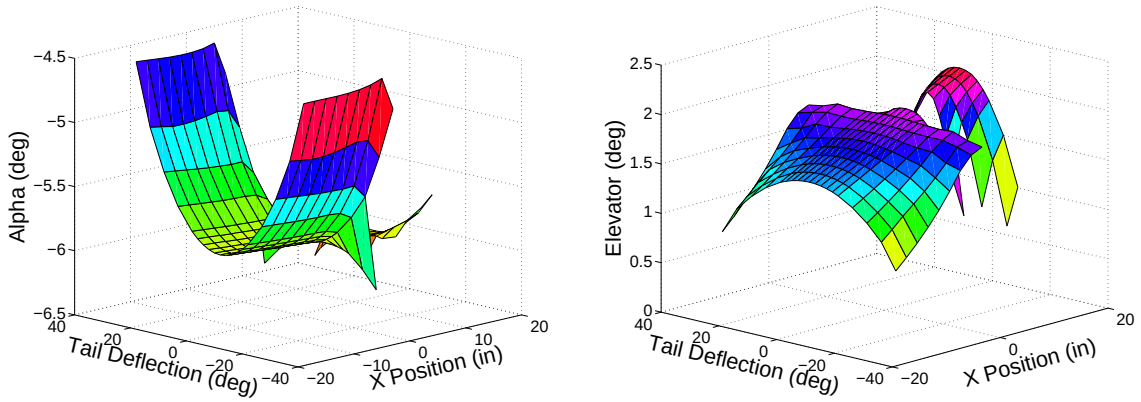

Figure 5-18. Angle of Attack and Elevator Deflection in a 45° Banked Turn

Aileron deflection has no relationship with the longitudinal placement of the vertical tail, but decreases linearly as the vertical tail is rotated in the positive direction (trailing

edge moving left), because the vertical tail deflection produces a roll moment when deflected that needs to be compensated by the ailerons.

Simultaneously, the model alters its sideslip angle to balance the yaw moments produced by the vertical tail's deflection. As expected, the sideslip angle roughly follows the tail deflection in magnitude and alternates directions depending on whether the vertical tail is located forward or aft of the model's center of mass.

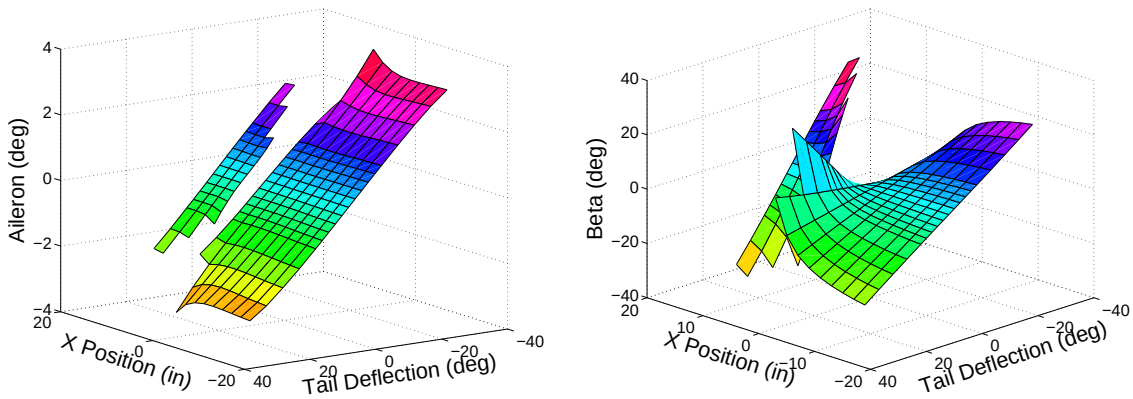

Figure 5-19. Aileron Deflection and Sideslip Angle in a 45° Banked Turn

The deflection of the control surfaces shown in Figure 5-18 and Figure 5-19 for the 45° banked turns are reasonable and well within the limits of existing actuators.

5.3.4 Static Stability

In banked turning flight, the same stability metrics are examined with respect to longitudinal position and angle of deflection of the vertical tail. It was observed previously that the vertical position of the vertical tail had little to no impact on turning performance metrics, but that both the longitudinal placement and deflection of the vertical tail did, so the trim dynamics are found at a variety of longitudinal positions and deflection angles to be able to weigh the performance benefits against the stability effects observed at these configurations.

The coefficient of pitching moment with respect to angle of attack as shown in Figure 5-20 exhibits a parabolic trend with respect to vertical tail deflections, centered

about a deflection angle of zero. Just as in steady level flight, the C_{m_α} shows a fairly linear relationship with respect to longitudinal position of the vertical tail, becoming increasingly stable as the vertical tail moves forward. Despite the trends seen in this important stability coefficient, the aircraft remains pitch stable with respect to angle of attack throughout all of the tested vertical tail longitudinal positions and deflection angles.

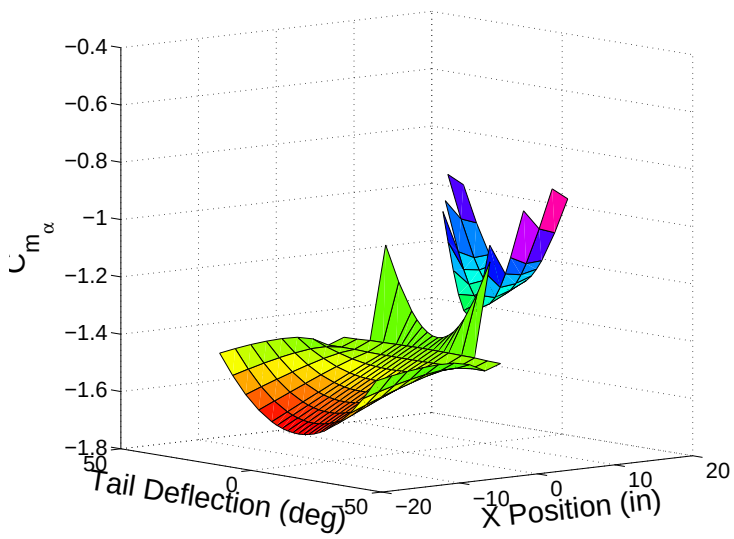

Figure 5-20. Pitch Moment Coefficient with respect to Angle of Attack in a 45° Banked Turn

The coefficient of rolling moment with respect to a sideslip angle, seen in Figure 5-21, shows distinct trends with respect to both longitudinal position and deflection of the vertical tail. This stability derivative increases in a roughly linear fashion as the vertical tail is moved forward, and, save for a discontinuity around small negative deflection angles, exhibits a roughly inverse parabolic shape with respect to vertical tail deflection angles. The inverse parabola from the latter trend is centered about a deflection angle of zero; thus, producing the highest stability derivative value for small tail deflections and the lowest value for large tail deflections, whether they are positive or negative. The trend with respect to longitudinal position of the vertical tail is also seen in the steady level flight analysis; and just as before, is probably an effect produced by complex aerodynamic

interactions. The trend with respect to tail deflections can probably be justified by noting two things. First, the vertical tail is, by nature, a destabilizing agent with respect to roll, that must be compensated by the wings. Second, as the vertical tail is deflected, less and less of its area is orthogonal to the component of the wind vector that is perpendicular to the aircraft's direction of travel. So, as the tail is increasingly deflected, it becomes a less destabilizing factor, causing the coefficient of rolling moment to decrease. The decrease in C_{l_β} makes the aircraft more roll stable with large vertical tail deflections, in addition to the increased roll stability produced by further aft vertical tail positions.

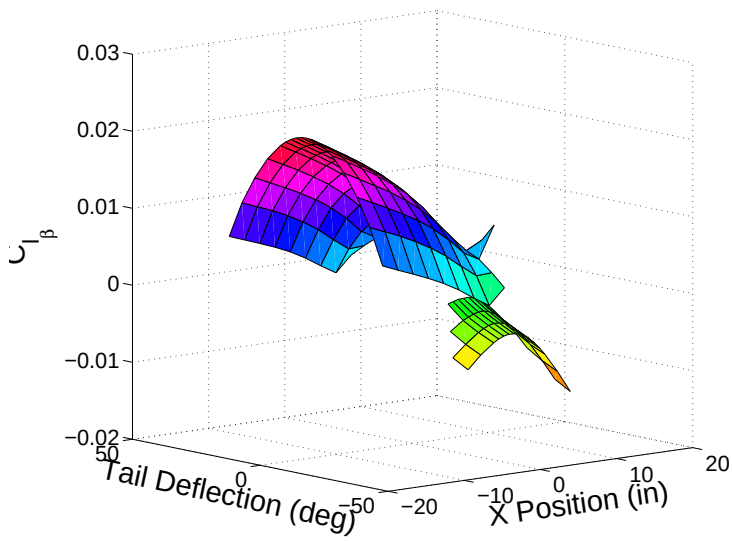

Figure 5-21. Roll Moment Coefficient with respect to Sideslip Angle in a 45° Banked Turn

The coefficient of yawing moment with respect to sideslip angle as shown in Figure 5-22 is nearly constant with respect to deflections of the vertical tail, but shows a linear correlation with respect to its longitudinal position. As explained before, it makes physical sense that this stability derivative would be highly dependent on the longitudinal position of the vertical tail, because the position impacts the tail's moment arm length, and thus, the moment that would be induced in the presence of a nonzero sideslip angle. Similar to the evidence from the steady level flight analysis, the aircraft is yaw-stable for

vertical tail positions sufficiently behind the aircraft's center of mass and increasingly unstable as the vertical tail moves forward.

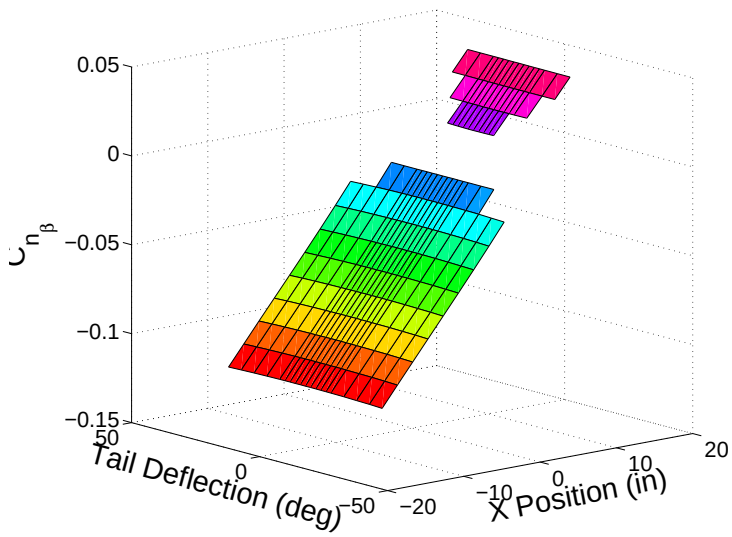

Figure 5-22. Yaw Moment Coefficient with respect to Sideslip Angle in a 45° Banked Turn

5.3.5 Control Effectiveness

The elevator experiences a reduction in its effect on pitch moment as the vertical tail deflects at large angles due to large changes in sideslip angle seen in Figure 5-19. These large changes in sideslip angle dramatically alter the flow over the elevator, thereby reducing its effect. The effect is more dramatic when the tail is located aft of the center of mass, because when the vertical tail is in front of the center of mass, it is also in front of the wing. The wing experiences the vertical tail sidewash when the vertical tail is forward of the wing; thus, reducing the local angle of sideslip on the wing.

The rudder's effect of yaw moment is linear with respect to the longitudinal position of the vertical tail. As explained before, this coefficient is highly dependent on the length of the moment arm between the aerodynamic center of the vertical tail and the center of mass of the aircraft. Vertical tail deflection has no impact on the effectiveness of the rudder in yaw moment.

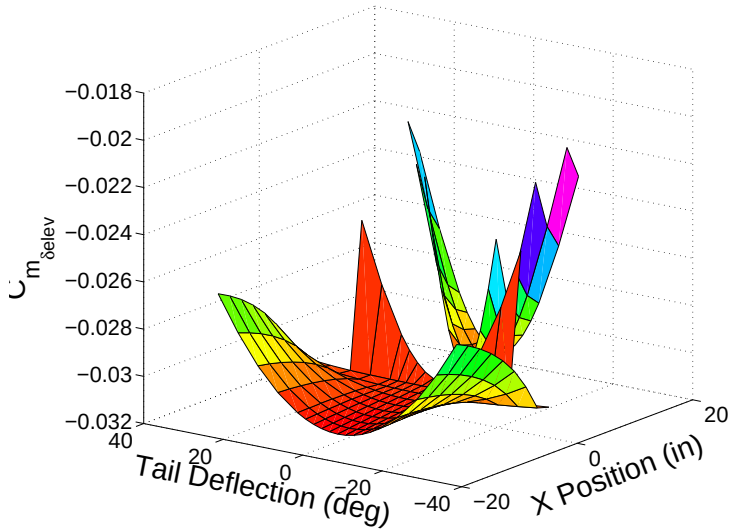

Figure 5-23. Elevator Control Effectiveness in a 45° Banked Turn

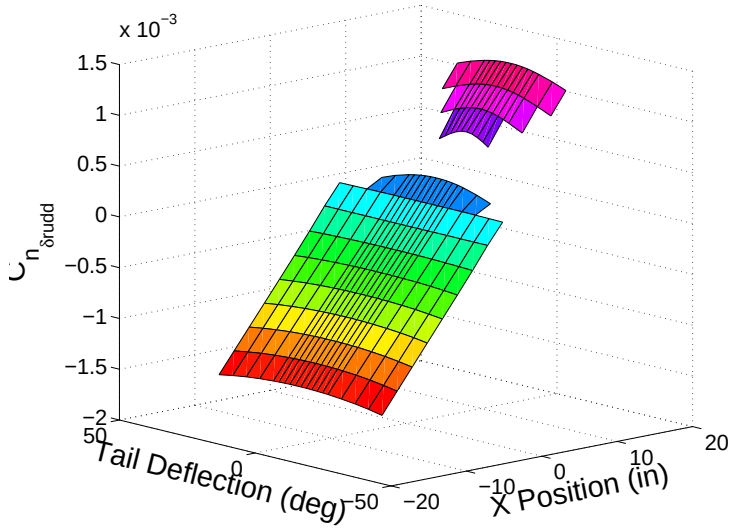

Figure 5-24. Rudder Control Effectiveness in a 45° Banked Turn

The ailerons lose control effectiveness when the vertical tail is deflected at large angles. The effect is even more pronounced when the tail is located aft of the vehicle's center of mass than when located farther forward. As seen in the elevator control effectiveness, this trend is the result of the large changes in sideslip angle seen in

Figure 5-19 when the vertical tail is deflected. These large changes in sideslip angle dramatically alter the flow over the ailerons, thereby reducing their effect.

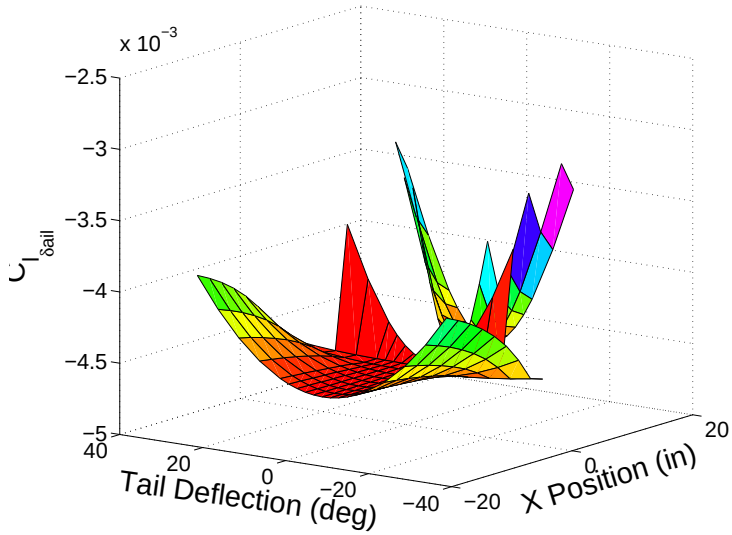

Figure 5-25. Aileron Control Effectiveness in a 45° Banked Turn

CHAPTER 6
RESULTS IMPLICATIONS

6.1 Biological Implications

Pterosaurs appear to have flown at larger angles of attack than conventional aircraft. Their large heads pushed their center of mass farther in front of the center of lift requiring significant wing twist and angle of attack to produce sufficient lift while simultaneously balancing the pitch moments.

Furthermore, pterosaurs likely swept their wings backward symmetrically to adopt a configuration that produces less drag, thereby allowing higher speeds, while at the same time improving its stability, making it easier to compensate for disturbances in the air on the windy coastlines of prehistoric Pangaea. It is interesting to note, that while the time constant decreases with backward wing sweep, the effectiveness of the rudder on yaw moment does not degrade.

Pterosaurs also would have used asymmetric wing morphing to enable them to look at a target of interest, while still maintaining their desired flight path. The pterosaur model shows the ability to balance yaw moments using a combination of head deflection, sideslip angle, and asymmetric wing sweep; thus, pterosaur had greater freedom in choosing its desired line of sight, flight direction, and flight dynamics.

The aerodynamic effects of Tapejara's cranial crest can not be overstated. In the presence of asymmetric wing sweep, the head is responsible for a 30% increase in drag, as shown in Figures 4-17 and 4-18. The crest also has a unique relationship with the wing sweep morphing that *Tapejara* could manipulate, as seen in the increases in control effectiveness throughout all run conditions, both steady level and turning. *Tapejara*'s crest could even be used in conjunction with wing sweep morphing to improve turning radius and turn rate.

6.2 Aircraft Implications

The trim flight conditions during straight-and-level flight are not influenced by the position of the rudder. As expected, the rudder is not required to trim the vehicle at conditions that do not involve an angle of sideslip.

The characteristics of a turn are obviously critical to agile maneuvering. In particular, a smaller radius of turn and correspondingly higher rate of turn can directly correlate to operating amongst denser obstacles. This turn radius is actually proportional to the square of the velocity and the inverse of the g-factor loading as shown in Equation 2–25.

The vertical tail has a significant effect on turning; consequently, varying the location of that tail will vary the turn characteristics. This effect is shown by computing the aerodynamics for a vehicle during a 45° turn. The resulting data for turn radius, shown in Figure 5-15, shows the influence of both position and rotation of the vertical tail. In this case, a vertical tail placed forward of the vehicle's center of mass is clearly shown to lower the turn radius as compared to the traditional configuration of a vertical tail placed far behind the center of mass. This data indicates that a vehicle with a variable-placement vertical tail could maneuver in less airspace and thus operate in more constrained environments than a traditional configuration.

The variations in turn radius result from associated variations in both velocity and turn rate. These parameters are shown in Figure 5-16 for a range of locations and angles of the vertical tail. As expected, the configurations with a vertical tail over the head and in front of the center of gravity are able to reduce the velocity and increase the turn rate.

A feature of note in Figure 5-15 that correlates with Figure 5-16 is the symmetry with respect to angle. Essentially, the results indicate that a similar turn radius can be achieved whether the tail is rotated into the turn or out of the turn. Such a result is somewhat unexpected; however, the symmetry arises by considering the angle of sideslip. A banked turn is often performed without any angle of sideslip but, as shown in Figure 5-19, this vehicle trims using a noticeable angle of sideslip. The use of sideslip actually induces more

drag and thus the vehicle can maintain trim at a slower velocity and consequently smaller radius.

The dynamic effects on yaw rotations are computed for these configurations. The plots shown in Figures 5-8 and 5-9 demonstrate the derivative of the coefficient of yaw moment with respect to both yaw rate and angle of sideslip. As expected, the plot of C_{n_r} is symmetric about perturbations to position while the plot of C_{n_β} is symmetric about perturbations to head angle. The value of C_{n_r} depends on the length of the moment arm and thus, is independent of fore or aft positioning. The value of C_{n_β} has a stabilizing restoring moment as long as the tail is aft of the center of gravity and is always destabilizing for any forward positioning.

Also note that the yaw effects produced by longitudinal variations in vertical tail placement affect the turning performance of the aircraft, but the roll effects produced by vertical variations in the tail placement do not. This result indicates that the key to producing more agile and mission capable aircraft lies not in rolling the aircraft, the way that large commercial jets turn, but in producing large yaw moments to spin the vehicle into its new direction.

REFERENCES

[1] Wlezien, R.W., Horner, G.C., McGowan, A.R., Padula, S.L., Scott, M.A., Silcox, R.J. and Simpson, J.O., "The Aircraft Morphing Program," *AIAA Structures, Structural Dynamics and Materials Conference*, AIAA Paper 98-1927, April 1998.

[2] Pendleton, E.W., Bessette, D., Field, P.B., Miller, G.D. and Griffin, K.E., "Active Aeroelastic Wing Flight Research Program: Technical Program and Model Analytical Development," *Journal of Aircraft*, Vol. 37, No. 4, July 2000, pp. 554-561.

[3] Wall, R., "Darpa Eyes Materials for Morphing Aircraft," *Aviation Week and Space Technology*, April 8, 2002.

[4] Abdulrahim, M., Garcia, H., Dupuis, J. and Lind, R., "Flight Characteristics of Wing Shaping for a Micro Air Vehicle with Membrane Wings," *International Forum on Aeroelasticity and Structural Dynamics*, IFASD-US-24, June 2003.

[5] Abdulrahim, M., Garcia, H., Ivey, G.F. and Lind, R., "Flight Testing a Micro Air Vehicle using Morphing for Aeroservoelastic Control," *AIAA Structures, Structural Dynamics and Materials Conference*, AIAA-2004-1674, April 2004.

[6] Garcia, H., Abdulrahim, M. and Lind, R., "Roll Control for a Micro Air Vehicle using Active Wing Morphing," *AIAA Guidance, Navigation and Control Conference*, AIAA-2003-5347, Aug. 2003.

[7] Grant, D.T., Abdulrahim, M. and Lind, R., "Flight Dynamics of a Morphing Aircraft utilizing Independent Multiple-Joint Wing Sweep," AIAA-2006-6505, Aug. 2006.

[8] Bowman, J., "Affordability Comparison of Current and Adaptive and Multifunctional Air Vehicle Systems," AIAA-2003-1713, April 2003.

[9] Gano, S.E. and Renaud, J.E., "Optimized Unmanned Aerial Vehicle with Wing Morphing for Extended Range and Endurance," AIAA-2002-5668, Sept. 2002.

[10] Bowman, J., Sanders B. and Weisshar, T., "Evaluating the Impact of Morphing Technologies on Aircraft Performance," AIAA-2002-1631, April 2002.

[11] Prock, B.C., Weisshaar, T.A. and Crossley, W.A., "Morphing Airfoil Shape Change Optimization with Minimum Actuator Energy as an Objective," AIAA-2002-5401, Sept. 2002.

[12] Rusnell, M.T., Gano, S.E., Perez, V.M., Renaud, J.E. and Batill, S.M., "Morphing UAV Pareto Curve Shift for Enhanced Performance," AIAA-2004-1882, April 2004.

[13] Secanell, M., Suleman, A. and Gamboa, P., "Design of a Morphing Airfoil for a Light Unmanned Aerial Vehicle using High-Fidelity Aerodynamic Shape Optimization," AIAA-2005-1891, April 2005.

[14] Khot, N.S., Eastep, F.E. and Kolonay, R.M., "Method for Enhancement of the Rolling Maneuver of a Flexible Wing," *Journal of Aircraft*, Vol. 34, No. 5, September-October 1997, pp. 673-678.

[15] Gern, F.H., Inman, D.J. and Kapania, R.K., "Structural and Aeroelastic Modeling of General Planform Wings with Morphing Airfoils," *AIAA Journal*, Vol. 40, No. 4, April 2002, pp. 628-637.

[16] Bae, J., Seigler, T.M., Inman, D.J. and Lee, I., "Aerodynamic and Aeroelastic Considerations of a Variable-Span Morphing Wing," *Journal of Aircraft*, Vol. 42, No. 2, March-April 2005, pp. 528-534.

[17] Love, M.H., Zink, P.S., Stroud, R.L., Bye, D.R. and Chase, C., "Impact of Actuation Concepts on Morphing Aircraft Structures," AIAA-2004-1724, April 2004.

[18] Chatterjee, S. and Templin, R.J., "Posture, Locomotion, and Paleoecology of Pterosaurs," *Geological Society of America Special Publication 376*, 2004, pp. 1-64.

[19] B. Etkin and L.D. Reid, Dynamics of Flight: Stability and Control, 3rd edition, 1996, John Wiley and Sons, Hoboken, NJ, pp. 15-127.

[20] J.D. Anderson, Jr., Introduction to Flight, 4th edition, 2003, McGraw Hill, Boston, MA, pp. 299-662.

[21] D.P. Raymer, Aircraft Design: A Conceptual Approach, 4th edition, 2006, AIAA, Reston, VA, pp. 467-560.

[22] D. Lay, Linear Algebra and Its Applications, 3rd edition, 2003, Addison Wesley, Boston, MA, pp. 302-303.

[23] Kehoe, J.J., Causey, R.S., Abdulrahim, M. and Lind, R., "Waypoint Navigation for a Micro Air Vehicle using Vision-Based Attitude Estimation," *The Aeronautical Journal*, Vol. 110, No. 1114, December 2006, pp. 821-829.

BIOGRAPHICAL SKETCH

Brian Christopher Roberts was born in Baltimore, Maryland in 1985. He grew up in Raleigh, North Carolina, where he graduated valedictorian of the class of 2003 from Jesse O. Sanderson High School. He returned to the state of his birth for college, where he attended the University of Maryland at College Park. During college, Brian spent one semester in Valencia, Spain at the Polytechnic University of Valencia before returning to Maryland to receive his Bachelor of Science degree in May of 2007. Brian graduated with Aerospace Honors for his research into ornithopters with Dr. James E. Hubbard, Jr. at the National Institute of Aerospace in Hampton, Virginia. He has been a graduate student at the University of Florida under the guidance of Dr. Rick Lind since June, 2007. He has researched pterosaur flight dynamics and their potential to inspire miniature aerial vehicle (MAV) design. During his time in the Flight Control Laboratory, Brian has helped to write proposals to Defense Advanced Research Projects Agency (DARPA) and the National Science Foundation (NSF). His proposal to NSF to study the effects of morphing MAV design on urban turbulence rejection was accepted, and he will spend the summer of 2009 in Melbourne, Australia pursuing that initiative. After receiving his Master of Science degree in May of 2009, Brian continues to pursue his MAV research interests to obtain his doctoral degree.